LBNL-51812

SOLUTIONS OF TEST PROBLEMS FOR DISPOSAL OF CO2 IN SALINE AQUIFERS

Karsten Pruess and Julio García

Earth Sciences Division, Lawrence Berkeley National Laboratory
Berkeley, CA 94720, U.S.A.

December 2002

This work was supported by the U.S. Department of Energy through the Office of Basic Energy Sciences (BES) and through the National Energy Technology Laboratory (NETL) under Contract No. DE-AC03-76SF00098.

ABSTRACT

This report presents detailed results for three flow problems involving CO2 migration in saline aquifers, that had been posed as part of an international code intercomparison study. Selected data for PVT properties of aqueous mixtures involving CO2 are given, and the dynamics of immiscible displacement of an aqueous phase by supercritical CO2 is discussed. Simulations were conducted with a version of the TOUGH2 general purpose reservoir simulator that includes a special property package for supercritical CO2. The results can serve as benchmarks for debugging numerical simulation models.

TABLE OF CONTENTS

LIST OF FIGURES vii

LIST OF TABLES ix

1. INTRODUCTION 1

2. PROBLEM 3. RADIAL FLOW FROM A CO2 INJECTION WELL 2
   - 2.1 Thermophysical Properties 2
   - 2.2 CO2 Injection into an Aquifer without Salinity 4
   - 2.3 CO2 Injection into a Saline Aquifer 8

3. PROBLEM 4. CO2 DISCHARGE ALONG A FAULT ZONE 12
   - 3.1 Thermophysical Properties 13
   - 3.2 Gravity Equilibration 13
   - 3.3 CO2 Displacement 15
   - 3.4 Numerical Artifacts 17
   - 3.5 Non-isothermal Variation 19

4. PROBLEM 7: CO2 INJECTION INTO A 2-D LAYERED BRINE FORMATION 23
   - 4.1 Thermophysical Properties 24
   - 4.2 Gravity Equilibration 25
   - 4.3 CO2 Injection 26

5. CONCLUDING REMARKS 34

ACKNOWLEDGEMENT 34

REFERENCES 35

Appendix A. Test Problem 3 37

Appendix B. Test Problem 4 39

Appendix C. Test Problem 7 41

LIST OF FIGURES

Figure 2.1 Schematic of test problem 3 2

Figure 2.2 Simulated gas saturation front (no salinity) 4

Figure 2.3 Simulated pressure (no salinity) 5

Figure 2.4 Simulated gas saturation (no salinity) 5

Figure 2.5 Simulated dissolved CO_2 mass fraction (no salinity) 6

Figure 2.6 TOUGH2 input file for the radial flow problem 7

Figure 2.7 Simulated pressure (15 wt.-% salinity) 9

Figure 2.8 Simulated gas saturation (15 wt.-% salinity) 9

Figure 2.9 Simulated dissolved CO_2 mass fraction (15 wt.-% salinity) 10

Figure 2.10 Simulated solid salt saturation (15 wt.-% salinity) 10

Figure 2.11 Simulated solid salt saturation using a finer grid near the injection well 11

Figure 3.1 Schematic of the fault zone model (a) and applied boundary conditions (b)..... 12

Figure 3.2 TOUGH2 input file for fault zone problem 14

Figure 3.3 Simulated results for fluxes and time steps versus time 16

Figure 3.4 Gas saturation and dissolved CO2 mass fractions at times of 10^7 and $2x10^7$ seconds 17

Figure 3.5 Pressure profiles at times of 10^7 and $2x10^7$ seconds 18

Figure 3.6 Transient evolution of pressures and gas saturations at a monitoring grid block, 372.5 m up the fault 19

Figure 3.7 Gas saturation profiles at 10^7 seconds for isothermal and non-isothermal conditions 20

Figure 3.8 Temperature profiles for a non-isothermal version of the problem at 10^7 seconds, and at the eventual steady state conditions 21

Figure 3.9 Enthalpy of pure CO2 as function of temperature and pressure, as calculated from the correlations of Altunin (1975) 22

Figure 4.1 Hydrostatic pressure profile prior to CO2 injection 27

Figure 4.2 TOUGH2 input file for CO2 injection into layered brine formation 28

Figure 4.3 Time stepping and gas saturation vs. time at the wellblock for the case with 3.2 wt.-% salinity 29

Figure 4.4 CO2 and salt mass fractions in the aqueous phase at the wellblock for the case with 3.2 wt.-% salinity 29

Figure 4.5 Gas saturation after 2 years of CO2 injection for the case with 3.2 wt.-% salinity 30

Figure 4.6 CO2 mass fraction dissolved in the aqueous phase after 2 years of CO2 injection for the case with 3.2 wt.-% salinity 30

Figure 4.7 Vertical profiles of gas saturation after two years at different distances from the left boundary for the case with 3.2 wt.-% salinity 31

Figure 4.8 Vertical profiles of gas saturation at 200 m distance from the left boundary for the case with 3.2 wt.-% salinity 32

Figure 4.9 Vertical profiles of gas saturation at 200 m distance from the left boundary after 2 years 33

Figure B.1 Schematic of the fault zone model (a) and applied boundary conditions (b) 39

Figure C.1 Schematic representation of geometry for CO2 injection in Utsira Formation 42

LIST OF TABLES

Table 2.1 Thermophysical properties at a temperature of 45 ˚C 3

Table 3.1 PVT properties at a temperature of 45 ˚C at selected pressures, as used in the TOUGH2 simulation 15

Table 3.2 CO2 inventory 17

Table 4.1 Grid increments (29 blocks in x from left to right; 34 blocks in y from bottom to top) 24

Table 4.2 PVT properties at a temperature of 37 ˚C for different salinities (no CO2) 24

Table 4.3 PVT properties at a temperature of 37 ˚C for two-phase fluid mixtures of water, CO2, and NaCl 25

Table 4.4 CO2 mass balances (in units of 10^6 kg) for injection into fresh water and saline systems 34

Table A.1 Hydrogeologic parameters 38

Table A.2 Initial conditions and injection specifications 38

Table C.1 Initial conditions and injection specifications 42

Table C.2 Hydrogeologic parameters 44

1. Introduction

Mathematical models and numerical simulation tools play an important role in evaluating the feasibility of geologic disposal of CO2, and reliable numerical simulators will be required for the design and safe operation of CO2 disposal facilities. The models must accurately represent the major physical and chemical processes that would be induced by injection of CO2 into potential disposal reservoirs. As a means of testing and evaluating numerical simulation codes we launched a code intercomparison study that featured eight prototypical simulation problems for CO2 disposal in saline aquifers, or oil and gas reservoirs (Pruess et al., 2000). Preliminary results of this study were presented at the Sixth International Conference on Greenhouse Gas Control Technologies (GHGT-6), held in October 2002 in Kyoto, Japan (Pruess et al., 2002a; Oldenburg et al., 2002), and a full report is available that compares results submitted by ten groups from six countries (Pruess et al., 2002b).

Here we present results obtained by LBNL for three of the numerical simulation problems in the intercomparison study that pertain to CO2 disposal in saline aquifers (brine formations). Our purpose is to present the simulations in greater detail than was possible in the full project report, to provide information that would be useful for benchmarking codes, and to give an expanded discussion on the behavior and dynamics of the disposal systems modeled. The analyses presented here address intercomparison problems #3 (radial flow from a CO2 injection well), #4 (CO2 discharge along a fault zone), and #7 (CO2 injection into a layered brine formation). For completeness we include the problem specifications that were given in the original report in appendices.

2. Problem 3. Radial Flow from a CO_2 Injection Well

This is a basic problem of CO_2 injection into a saline aquifer, examining two-phase flow with CO2 displacing (saline) water under conditions that may be encountered in brine aquifers at a depth of the order of 1.2 km. A CO_2 injection well fully penetrates a homogeneous, isotropic, infinite-acting aquifer of 100 m thickness (Figure 2.1). The problem was simulated using the TOUGH2 code (Pruess et al., 1999) with an enhanced version of the EWASG fluid property module (Battistelli et al., 1997) known as ECO2 (Pruess and García, 2002). Variations are limited to two cases, namely, with and without salinity. All runs are performed in isothermal mode at T = 45 ^{o}C with initial pressure P = 120 bar. The numerical grid is extended to a large distance of 100 km, so that the system would be infinite-acting for the time period simulated (10,000 days, 27.38 years). The well is modeled as a circular grid element of R = 0.3 m into which CO_2 is injected uniformly at a constant rate of 100 kg/s. Full specifications are given in Appendix A. A similar problem with slightly different specifications was recently studied by Pruess and García (2002).

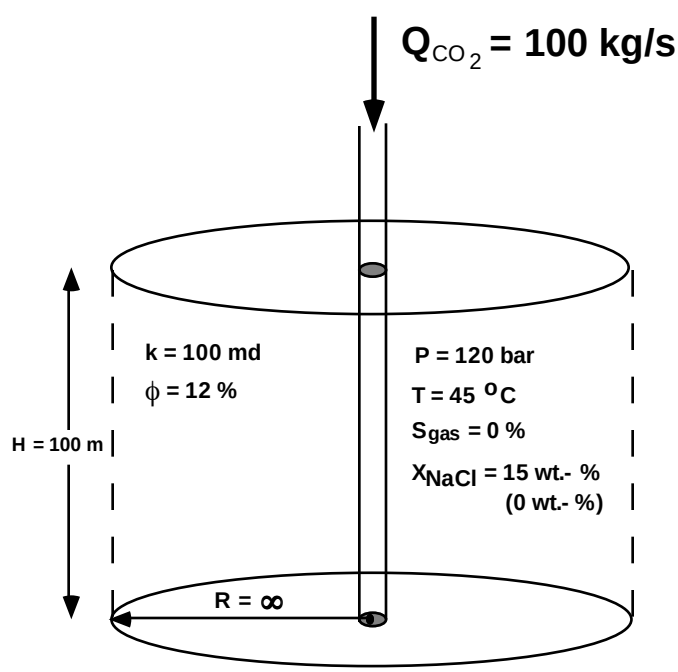

Figure 2.1 Schematic of test problem 3.

2.1 Thermophysical Properties

Representative fluid properties used in both simulations (with and without salinity) are given in Table 2.1. A summary of the thermophysical property model used is given in Pruess and García (2002). Pure fluid properties for water and CO_2 are represented by correlations of the International Formulation Committee (1967) and Altunin (1975), respectively. Following Battistelli et al. (1997),

Table 2.1 Thermophysical properties at a temperature of 45 ˚C.

Fluid phase / Pressure (bar)	120	160	200	240
pure water				
density (kg/m^3)	994.77	996.29	997.82	999.35
viscosity (Pa.s)	5.97778e-4	5.98341e-4	5.98929e-4	5.99540e-4
water with CO_2				
density (kg/m^3)	1005.70	1008.14	1010.07	1011.72
viscosity (Pa.s)	5.97778e-4	5.98341e-4	5.98929e-4	5.99540e-4
CO_2 mass fraction	5.1616e-2	5.6165e-2	5.8304e-2	5.9090e-2
gas				
density (kg/m^3)	658.57	760.89	813.49	850.14
viscosity (Pa.s)	5.16820e-5	6.56320e-5	7.45049e-5	8.15659e-5
water mass fraction	9.93985e-5	8.60323e-5	8.04694e-5	7.70001e-5
brine (water + 15 wt. % NaCl)				
density (kg/m^3)	1100.00	1101.53	1103.07	1104.61
viscosity (Pa.s)	8.28519e-4	8.29299e-4	8.30113e-4	8.30961e-4
brine with CO_2				
density (kg/m^3)	1103.54	1105.36	1107.01	1108.57
viscosity (Pa.s)	8.28519e-4	8.29299e-4	8.30113e-4	8.30961e-4
CO_2 mass fraction	2.5234e-2	2.7494e-2	2.8558e-2	2.8950e-2

aqueous phase (brine) density is calculated as a function of temperature, pressure and salinity from a correlation given by Phillips et al. (1981). Halite (NaCl) solubility is calculated from an equation due to Potter quoted in Chou (1987), and salinity effects on vapor pressure are represented with a correlation due to Haas (1976). CO_2 dissolution in aqueous phase is modeled using an extended version of Henry's law that includes a fugacity coefficient and a Poynting correction factor. Henry's coefficient is a function of temperature and mole fraction of salt dissolved in the aqueous phase. Water partitioning into the gas phase is modeled as an evaporation process (see additional details in section 3.1). Changes in aqueous phase density from CO_2 dissolution have a small impact on simulated system behavior, but were included using a correlation developed by García (2001). No allowance is presently made for dependence of aqueous phase viscosity on dissolved CO_2.

2.2 CO_2 Injection into an Aquifer without Salinity

Figure 2.2 shows the evolution of the gas saturation front up to a time of 10,000 days. An important advantage of the radial flow problem considered here is that it admits a similarity solution. Specifically, the solution depends on radial distance R and time t only through the similarity variable $\xi = R^2/t$, even when taking into account all the non-linearities due to PVT properties and two-phase flow (O'Sullivan, 1981; Doughty and Pruess, 1992). The space and time discretization employed for finite difference simulation will violate the rigorous R^2/t invariance, so that the similarity property will be maintained only approximately. Accuracy of the numerical simulation can be checked by plotting the results as a function of the similarity variable R^2/t. Figure 2.3 shows the results for pressure as a function of the similarity variable. Simulated results are presented for four different times (t = 30, 100, 1000, 10000 days) and two fixed locations (R = 25.25, 1011 m). The agreement is good, confirming the approximate preservation of the similarity property in the numerical solution. Figures 2.4 and 2.5 show simulated results for gas saturation and dissolved CO_2 mass fraction as a function of the similarity variable. Gas saturation results show three distinct regions emerging from the CO_2 injection process. The first region with $R^2/t \leq 5\times10^{-7}$ m^2/s corresponds to a zone where complete dry-out of aqueous phase has occurred. This region is followed by an intermediate region extending to $R^2/t \approx 10^{-2}$ m^2/s where liquid and gas phases coexists. Finally, there is an outer region with $R^2/t \geq 10^{-2}$ m^2/s in which single-phase liquid conditions prevail. The TOUGH2 input file used for the simulation is shown in Figure 2.6.

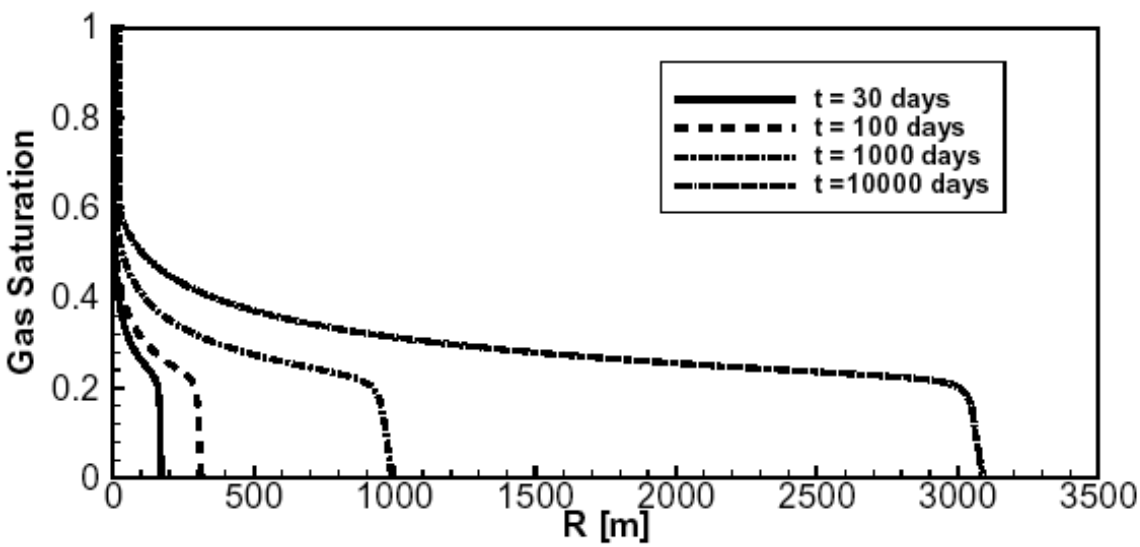

Figure 2.2 Simulated gas saturation front (no salinity).

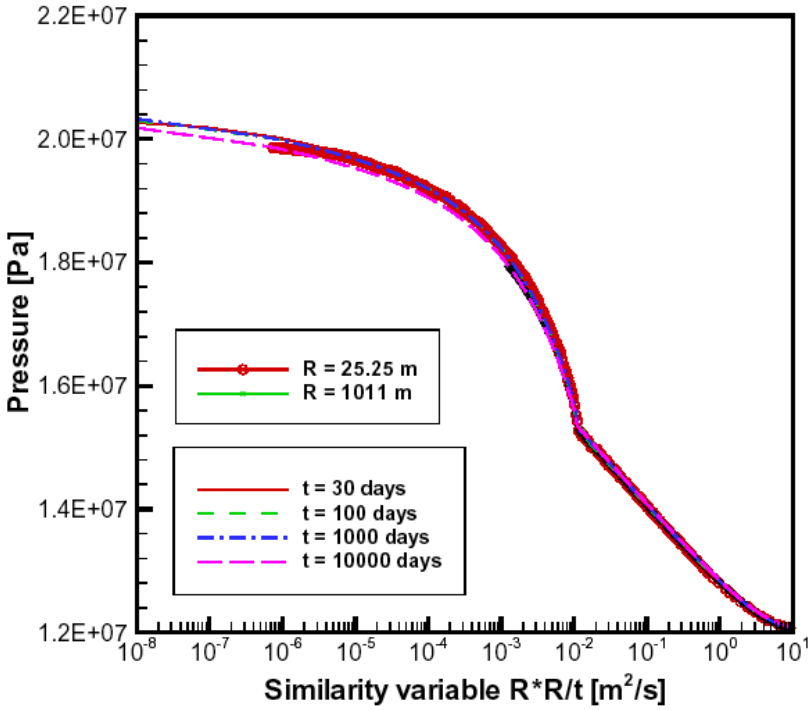

Figure 2.3 Simulated pressure (no salinity).

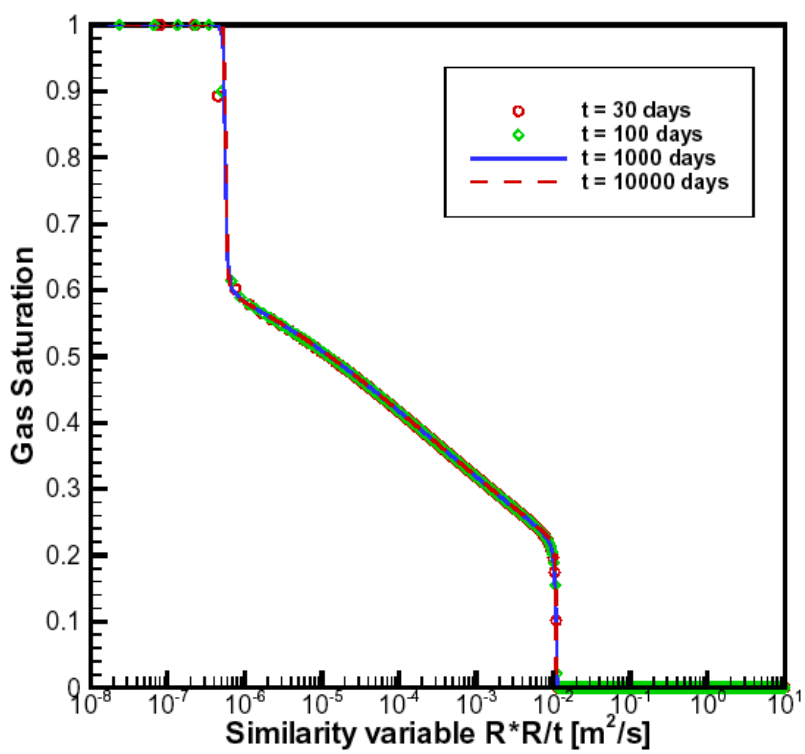

Figure 2.4 Simulated gas saturation (no salinity).

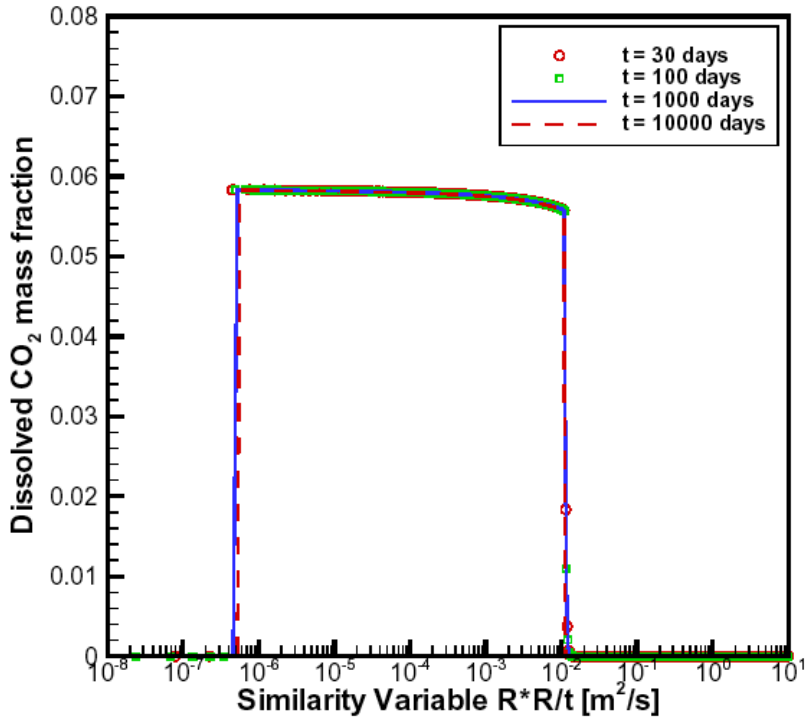

Figure 2.5 Simulated dissolved CO_2 mass fraction (no salinity).

```
*jgr1d.t2i* ... 1-D radial flow problem for CO2 injection into aquifer
MESHMAKER1----*----2----*----3----*----4----*----5----*----6----*----7----*----8
RZ2D
RADII
    1
        0.
EQUID
    1             .3
LOGAR
  200           1.E3
LOGAR
  100           3.E3
LOGAR
  100           1.E4
LOGAR
   34           1.E5
LAYER----1----*----2----*----3----*----4----*----5----*----6----*----7----*----8
    1
      100.

ROCKS----1----*----2----*----3----*----4----*----5----*----6----*----7----*----8
SAND     2  2600.e00       .12  100.e-15  100.e-15  100.e-15      2.51      920.
   4.5e-10
    7           .457       .30        1.       .05
    7           .457       .00    5.1e-5      1.e7      .999

MULTI----1----*----2----*----3----*----4----*----5----*----6----*----7----*----8
    3    3    3    6
SELEC....2....3....4....5....6....7....8....9...10...11...12...13...14...15...16
    1                                        1    0    0    2    2    0    0    2
        .8   .8
     ..... IE(16) = 2 chooses CO2, = 3 is for methane.
SOLVR----1----*----2----*----3----*----4----*----5----*----6----*----7----*----8
5  Z1   O0    8.0e-1    1.0e-7
START----1----*----2----*----3----*----4----*----5----*----6----*----7----*----8
----*----1 MOP: 123456789*123456789*1234 ---*----5----*----6----*----7----*----8
PARAM----1----*----2----*----3----*----4----*----5----*----6----*----7----*----8
   1 999     999 000300000000  4    3
            8.64E+08       -1.
        1.
     1.E-5     1.E00
              120.e5                 .15                 0.0                 45.
FOFT ----1----*----2----*----3----*----4----*----5----*----6----*----7----*----8
A1 49              1 .1745E+04 .2685E+03           .2570E+02          -.6500E+01
A12 2              1 .3080E+08 .4738E+07           .1080E+04          -.6500E+01

GENER----1----*----2----*----3----*----4----*----5----*----6----*----7----*----8
A1  1inj 1                        COM3       100.

INCON----1----*----2----*----3----*----4----*----5----*----6----*----7----*----8

TIMES----1----*----2----*----3----*----4----*----5----*----6----*----7----*----8
    4
 2.592E+06  8.64E+06  8.64E+07  8.64E+08
ENDCY----1----*----2----*----3----*----4----*----5----*----6----*----7----*----8
```

Figure 2.6 TOUGH2 input file for the radial flow problem.

2.3 CO_2 Injection into a Saline Aquifer

The presence of salt in the system induces additional processes, particularly salt precipitation near the injection well. The volume fraction of precipitated salt in the original pore space ϕ_0 is termed "solid saturation", and denoted by S_s. A fraction $\phi_0 S_s$ of reservoir volume is occupied by precipitate, while the remaining void space $\phi_f = \phi_0(1-S_s)$ is available for fluid phases; ϕ_f is referred to as "active flow porosity." The reduction of pore space reduces the permeability of the medium. The current version of ECO2 inherited the models for permeability reduction from the EWASG module (Battistelli et al., 1997) of which it is a descendant. The change of permeability due to porosity reduction is a complex process and a variety of models have been proposed in the literature (Verma and Pruess, 1988; Pape et al., 1999). To facilitate the comparison of the results presented here with other codes, the permeability reduction capability implemented in ECO2 was turned off. Nevertheless one must be aware of the possible implications of this simplification. A similar simulation presented in Pruess and García (2002) showed that a modest amount of precipitation of S_s = 2 % produced a reduction in permeability of 18 %.

Simulated results (Figs. 2.7, 2.8, 2.9) show that the overall behavior is very similar to the simulation run without salinity. As expected, the three distinct regions developed during CO_2 injection occur at about the same R^2/t locations. A 10 % higher pressure buildup occurs in the vicinity of the injection well, due to the larger viscosity of brine as compared to fresh water. Comparing Fig. 2.9 with Fig. 2.5 it is seen that the dissolution of CO_2 in the aqueous phase is reduced by 50 % due to salinity effects ("salting out").

The figures for pressure, saturation and dissolved CO_2 mass fraction demonstrate that the similarity property is well maintained. The results for solid saturation show considerable scatter at small values of R^2/t where discretization errors are significant (Fig. 2.10). Salt precipitation occurs only in the vicinity of the injection well (first 20 meters). In order to reduce discretization errors when calculating solid salt saturation, we performed another simulation with a finer grid, using small increments of constant ΔR = 0.05 m near the injection point. This prevents large jumps in solid saturation at elements near the injection well, and provides excellent preservation of the similarity property (Fig. 2.11).

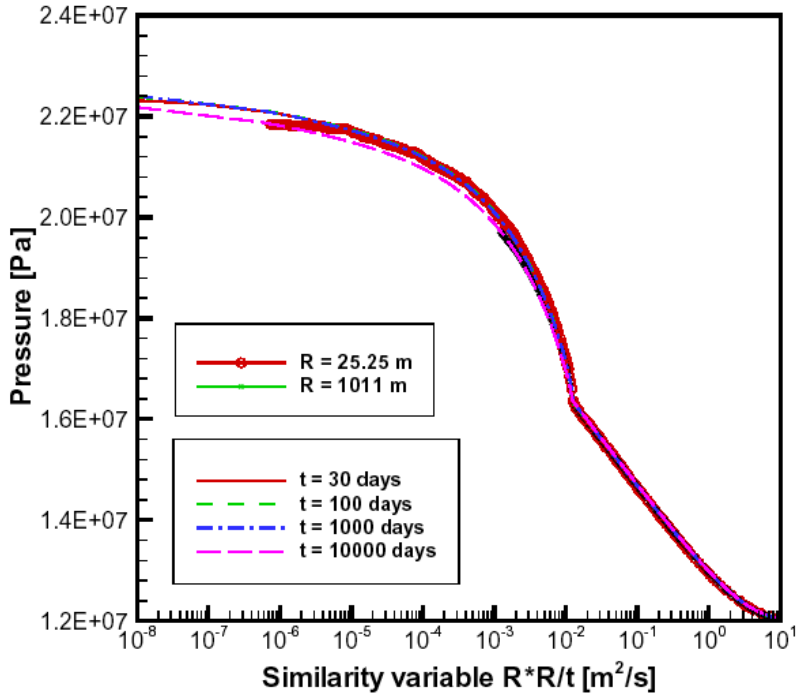

Figure 2.7 Simulated pressure (15 wt.-% salinity).

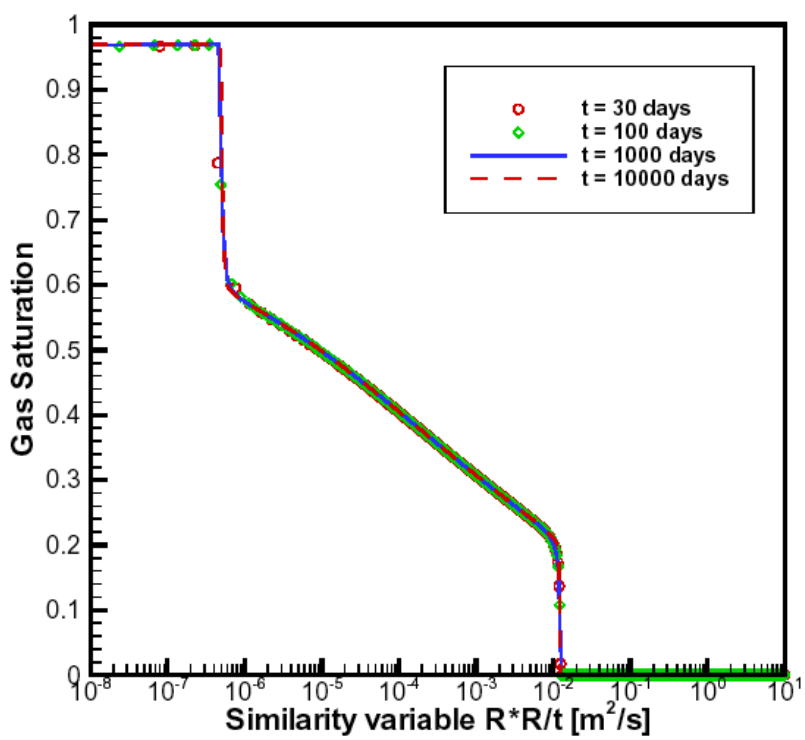

Figure 2.8 Simulated gas saturation (15 wt.-% salinity).

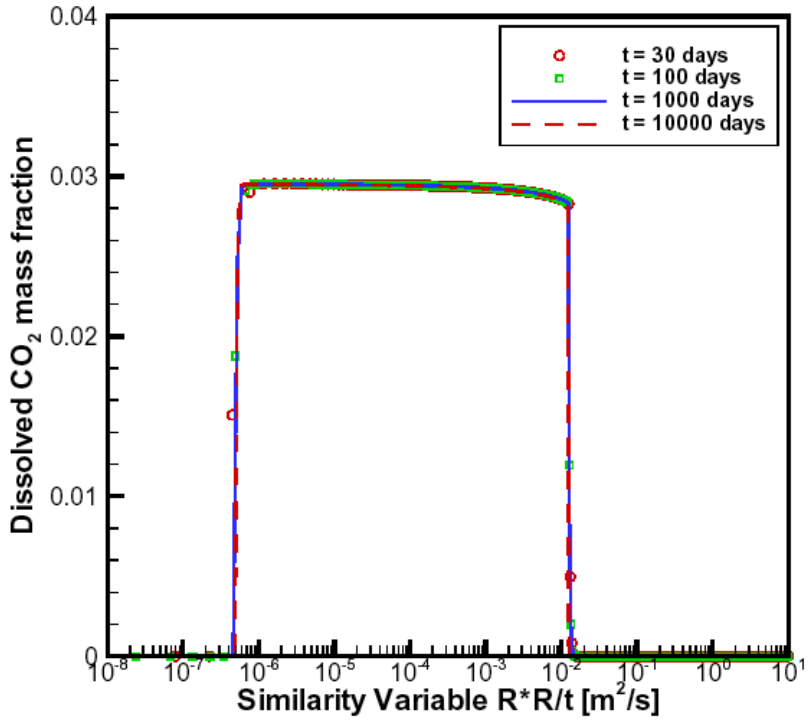

Figure 2.9 Simulated dissolved CO_2 mass fraction (15 wt.-% salinity).

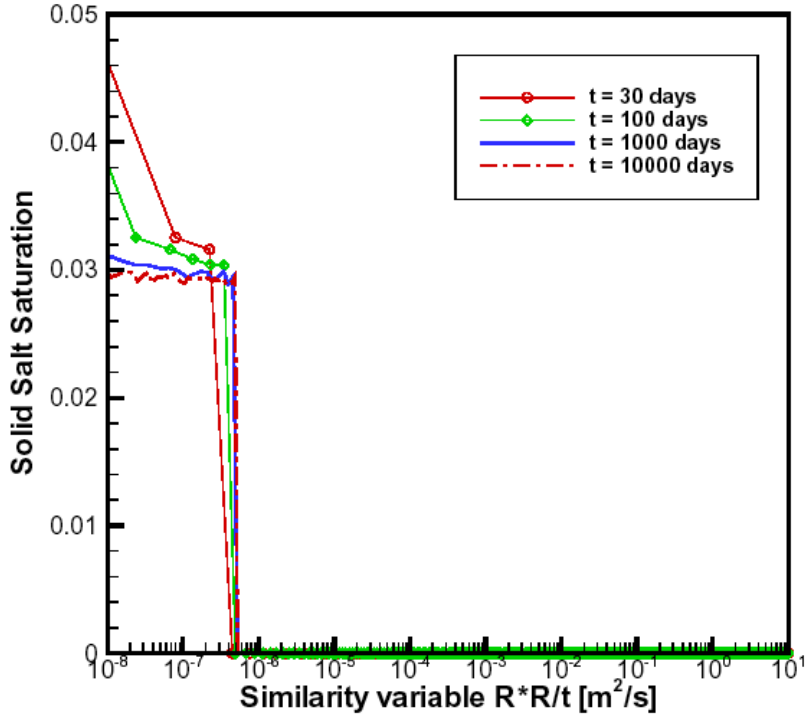

Figure 2.10 Simulated solid salt saturation (15 wt.-% salinity).

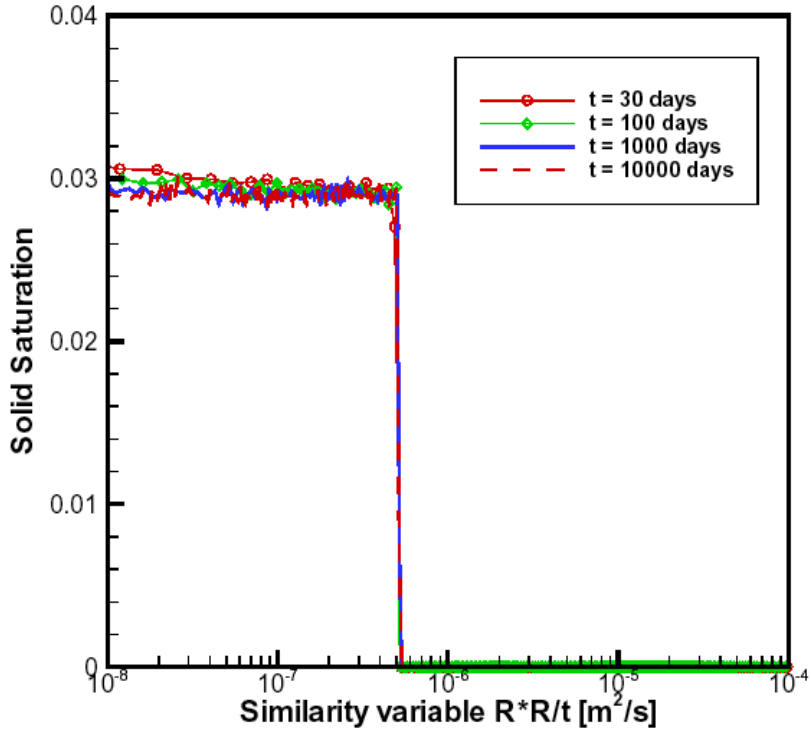

2.11 Simulated solid salt saturation using a finer grid near the injection well.

3. Problem 4. CO2 Discharge Along a Fault Zone

The amounts of CO2 that would need to be disposed of at fossil-fueled power plants are very large. A coal-fired plant with a capacity of 1,000 MWe generates approximately 30,000 tonnes of CO2 per day (Hitchon 1996). When disposed of into brine formations, CO2 injection plumes would over time extend to large distances of the order of ten kilometers or more, making it likely that geologic discontinuities such as faults and fractures will be encountered, with an associated potential for CO2 losses from the primary disposal aquifer. CO2 leaks through caprock discontinuities have a potential for self-enhancement, because pressures can actually decrease and/or flow rates increase as escaping CO2 creates a pathway towards shallower strata. It may be possible for a runaway process to develop where an initially "small" leak may accelerate to the point of a catastrophic, eruptive failure of a CO2 disposal system, that could result in major CO2 discharge and damage at the land surface (Pruess and García, 2002).

Migration of CO2 along a water-saturated fault zone would be subject to gravitational and viscous instabilities, and would likely involve complex two- and three-dimensional flow effects. As a first approximation to this kind of problem, we consider here a highly simplified situation in which a potential CO2 leakage path is modeled as a 1-D column (Fig. 3.1). Problem specifications are given in Appendix B.

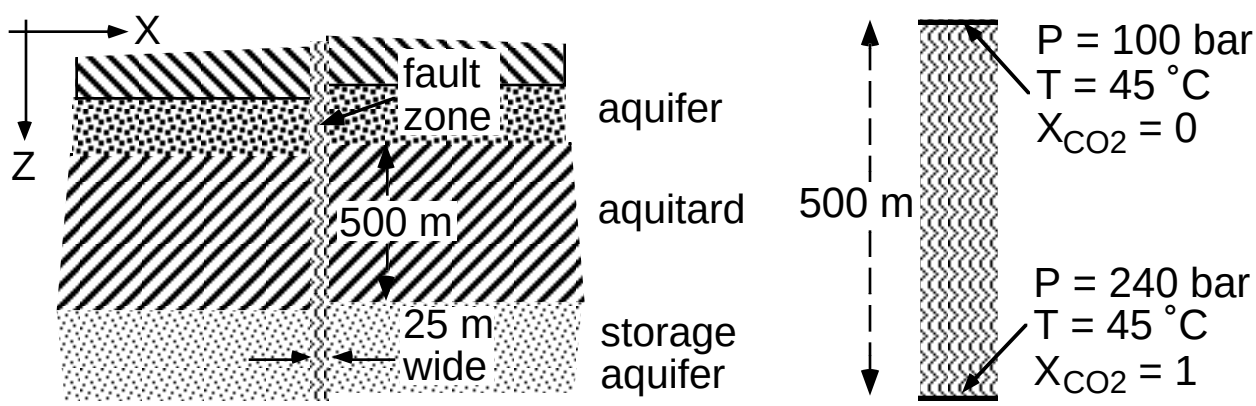

(a) (b)

Figure 3.1 Schematic of the fault zone model (a) and applied boundary conditions (b).

This problem was simulated with the TOUGH2 code (Pruess et al., 1999), using an enhanced version of the EWASG fluid property module (Battistelli et al., 1997) known as "ECO2" (Pruess and García, 2002). The problem is run in two segments. A first run segment obtains gravity equilibrium relative to a pressure of 100 bar prescribed at the top boundary. The gravity-equilibrated conditions obtained are used as initial conditions in a second run segment, where conditions of P = 240 bar and X_{CO2} = 1 are maintained at the lower boundary. All runs are

performed for pure water (no salinity) in isothermal mode at T = 45 ˚C. A length of 1 m of fault zone is simulated and a constant vertical grid spacing of 5 m is specified. The TOUGH2 input file for the problem is shown in Fig. 3.2.

3.1 Thermophysical Properties

Representative fluid properties used in the simulation are given in Table 3.1. Water properties are represented, within experimental uncertainty, by the steam table equations published by the International Formulation Committee (1967). Properties of pure CO2 are obtained from the correlations of Altunin (1975), as implemented in a computer program kindly provided to us by V.I. Malkovsky of IGEM, Moscow (private communication, 1999). The Altunin correlations are used to tabulate CO2 density and viscosity vs. temperature and pressure, with increments of $\Delta T = 2$ ˚C, $\Delta P = 4$ bar. During a simulation TOUGH2 performs interpolation from these tables. CO2 dissolution in the aqueous phase is modeled with an extended version of Henry's law that includes fugacity effects (Spycher and Reed, 1988) and a Poynting correction for CO2 solubility (Prausnitz et al., 1986), with a molar volume of 32.1 cm^3/mole (Spycher et al., 2002). No allowance is presently made for changes in water density and viscosity from CO2 dissolution. Water partitioning into the CO2-rich (gas) phase is modeled as an evaporation process, as follows. In two-phase conditions, water partial pressure in the gas phase is assumed equal to saturated vapor pressure, $P_v = P_{sat}(T)$, and additivity of pressures is assumed so that $P_{gas} = P_{CO2} + P_v$. This model underestimates the (small) water content of the gas phase; a more accurate correlation has recently been developed but has not yet been implemented into TOUGH2/ECO2 (Spycher et al., 2002). A summary of the thermophysical property model used here is given in Pruess and García (2002).

3.2 Gravity Equilibration

Pore compressibility is set to 0 in this part of the simulation, so that porosity remains a constant 35 % throughout as fluid pressures change. A tight convergence tolerance of RE1 = 1.e-10 is used. After 22 time steps and a simulation time of $t = 4.72 \times 10^9$ seconds an accurate hydrostatic equilibrium is obtained, with maximum pore velocities of 2×10^{-19} m/s. Pressure in the lowest grid block, 2.5 m above the lower boundary, is computed as 148.56 bar.

```
*r1dv* ... 1-D vertical column; CO2 migration up a fault zone
ROCKS----1----*----2----*----3----*----4----*----5----*----6----*----7----*----8
fault    2  2600.e00       .35  100.e-15  100.e-15  100.e-15      2.51      920.
   4.5e-10
    7           .457       .30        1.       .05
    7           .457       .00    5.1e-5      1.e7      .999
CO2in    2  2600.e00       .35  100.e-15  100.e-15  100.e-15      2.51      920.
   4.5e-10
    7           .457       .30        1.       .05
    8

MULTI----1----*----2----*----3----*----4----*----5----*----6----*----7----*----8
    3    3    3    6
SELEC....2....3....4....5....6....7....8....9...10...11...12...13...14...15...16
    1                                          0    0    0    2    0    0    2
        .8   .8
     ..... IE(16) = 2 chooses CO2, = 3 is for methane.
SOLVR----1----*----2----*----3----*----4----*----5----*----6----*----7----*----8
5  Z1   O0    8.0e-1    1.0e-7
START----1----*----2----*----3----*----4----*----5----*----6----*----7----*----8
----*----1 MOP: 123456789*123456789*1234 ---*----5----*----6----*----7----*----8
START----1----*----2----*----3----*----4----*----5----*----6----*----7----*----8
PARAM----1----*----2----*----3----*----4----*----5----*----6----*----7----*----8
   11000    9999 000 00000000  4    3
                          -1.                          9.81
        1.        9.      9.e1      9.e2
     1.E-5     1.E00
              100.e5                 .00                 0.0                 45.
INDOM----1----*----2----*----3----*----4----*----5----*----6----*----7----*----8
CO2in
              240.e5                 .00                 1.0                 45.

ELEME----1----*----2----*----3----*----4----*----5----*----6----*----7----*----8
flt 0   99    1fault      125.
ina
top 0
bot 0          CO2in

CONNE----1----*----2----*----3----*----4----*----5----*----6----*----7----*----8
bot 0flt 0                   3     1.e-3       2.5       25.       -1.
flt 0flt 1   98    1    1    3       2.5       2.5       25.       -1.
flt99top 0                   3       2.5     1.e-3       25.       -1.

COFT ----1----*----2----*----3----*----4----*----5----*----6----*----7----*----8
bot 0flt 0                   3     1.e-3       2.5       25.        1.
flt99top 0                   3       2.5     1.e-3       25.        1.

FOFT ----1----*----2----*----3----*----4----*----5----*----6----*----7----*----8
flt74
flt75

GENER----1----*----2----*----3----*----4----*----5----*----6----*----7----*----8

TIMES----1----*----2----*----3----*----4----*----5----*----6----*----7----*----8
    8
      1.E5      1.e6      1.e7      2.e7      1.e8      1.e9     1.e10     1.e11
ENDCY----1----*----2----*----3----*----4----*----5----*----6----*----7----*----8
```

Figure 3.2 TOUGH2 input file for fault zone problem.

Table 3.1. PVT properties at a temperature of 45 ˚C at selected pressures, as used in the TOUGH2 simulation.

P (bar) / fluid phase	120	160	200	240
pure water				
density (kg/m3)	994.768	996.292	997.821	999.354
viscosity (Pa s)	5.97778e-4	5.98341e-4	5.98929e-4	5.99540e-4
water with CO2				
density (kg/m3)	994.768	996.292	997.821	999.354
viscosity (Pa s)	5.97778e-4	5.98341e-4	5.98929e-4	5.99540e-4
CO2 mass fraction	5.22541e-2	5.70921e-2	5.95094e-2	6.05605e-2
gas				
density (kg/m3)	658.574	760.891	813.493	850.145
viscosity (Pa s)	5.16820e-5	6.56320e-5	7.45049e-5	8.15659e-5
water mass fraction	9.93985e-5	8.60323e-5	8.04694e-5	7.70001e-5

3.3 CO2 Displacement

Capillary pressure parameters were adjusted so that maximum Pcap is 10^7 Pa, and Pcap vanishes for small gas saturations of $S_g \leq 0.001$. These and other simulation parameters can be seen from the TOUGH2 input deck, Fig. 3.2.

The simulated evolution of the system proceeds through four stages (Fig. 3.3). In stage 1, CO2 enters the first grid block above the lower boundary, evolving a gas phase there and causing rapid pressurization that migrates up the fault. Stage 1 ends at approximately 10^4 seconds when the pressure pulse reaches the top of the fault, causing outflow of water to commence. During the subsequent stage 2 the CO2 displacement front migrates up the fault until, after about $3x10^7$ seconds, the front reaches the top. At this time CO2 discharge from the fault begins, while water discharge declines to small values because capillary effects reduce the effective pressure gradient for the aqueous phase at the top of the fault. Stage 3 lasts from $3x10^7$ to $2x10^{10}$ seconds, and is characterized by single-phase gas outflow from the fault. Water continues to be removed by evaporation into the flowing gas phase, causing gas relative permeabilities and flow rates to increase. As gas saturations increase capillary pressures get stronger, and at $1.16x10^{10}$ seconds the effective pressure gradient for the aqueous phase at the top of the fault reverses, leading to downflow of water from the top boundary at very small rates. Eventually the entire flow system

dries out, and in stage 4 we have a steady single-phase gas flow up the fault. TOUGH2 recognizes a steady state, and the simulation terminates after 486 time steps and a simulation time of 2.552×10^{13} seconds.

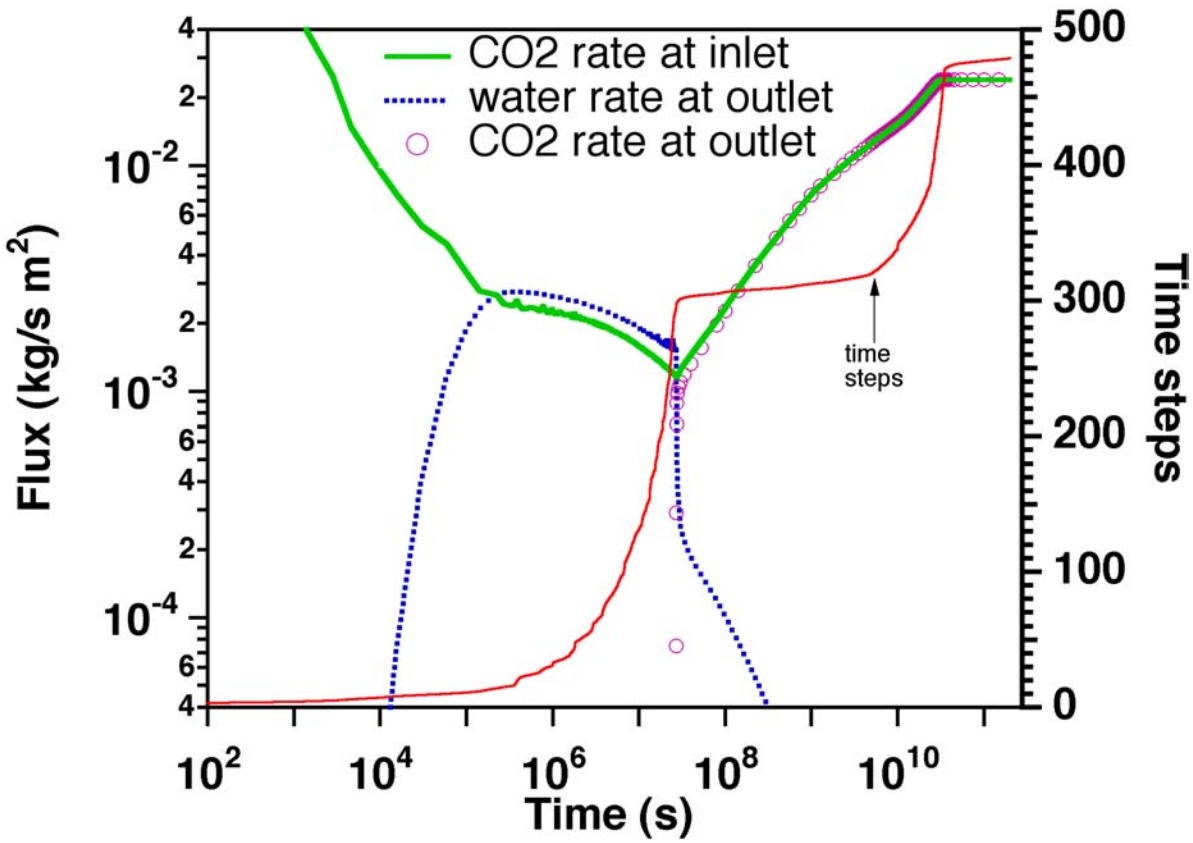

Figure 3.3 Simulated results for fluxes and time steps versus time.

Simulation progress and time stepping reflect non-linearities of the flow processes. Many relatively small time steps are required toward the end of stage 2 as the two-phase front approaches the upper boundary (Fig. 3.3). Smaller time steps again occur towards the end of stage 3 when the dryout front approaches the top boundary.

Profiles of gas saturations and CO2 mass fractions dissolved in the aqueous phase are shown in Fig. 3.4 at times of 10^7 and 2×10^7 seconds. Dissolved CO2 mass fractions range from 5.5 % near the top of the two-phase zone to 6 % near the bottom of the fault. Fugacity and Poynting corrections for CO2 dissolution have very substantial effects; without such corrections, dissolved CO2 mass fraction would be in excess of 18 %. Pressure profiles at times of 10^7 and 2×10^7 seconds are given in Fig. 3.5. The change in slope marks the transition from two-phase conditions below to single-phase conditions above. The pressure gradient in the two-phase zone is

larger than in the single-phase region, indicating that mobility loss from relative permeability effects dominates over mobility gain from the lower viscosity of CO2 as compared to water. Results for the simulated CO2 inventory of the system at t = 10^7 and $2x10^7$ seconds are given in Table 3.2.

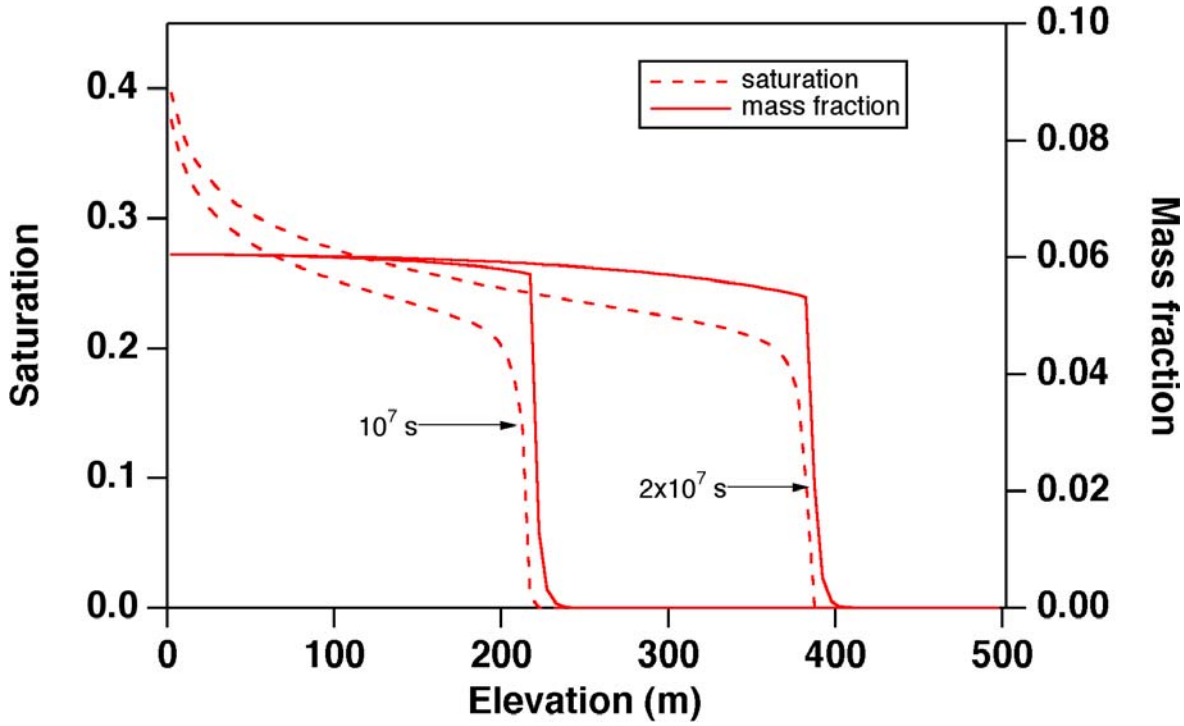

Figure 3.4 Gas saturation and dissolved CO2 mass fractions at times of 10^7 and $2x10^7$ seconds.

Table 3.2. CO2 inventory.

	10^7 seconds	$2x10^7$ seconds
gas phase	396.706 tonnes	690.489 tonnes
liquid phase	86.795 tonnes	147.934 tonnes
total	483.502 tonnes	838.424 tonnes

3.4 Numerical Artifacts

Fig. 3.6 shows the transient evolution of pressures and gas saturations at a monitoring grid block that is located at an elevation of 372.5 m up the fault. Pressures are seen to go through rapid variations as the grid block makes a transition from single-phase to two-phase conditions. The pressure transients are mostly spurious effects that arise from space discretization and can be understood as follows. As long as the monitoring block remains in single-phase conditions, all

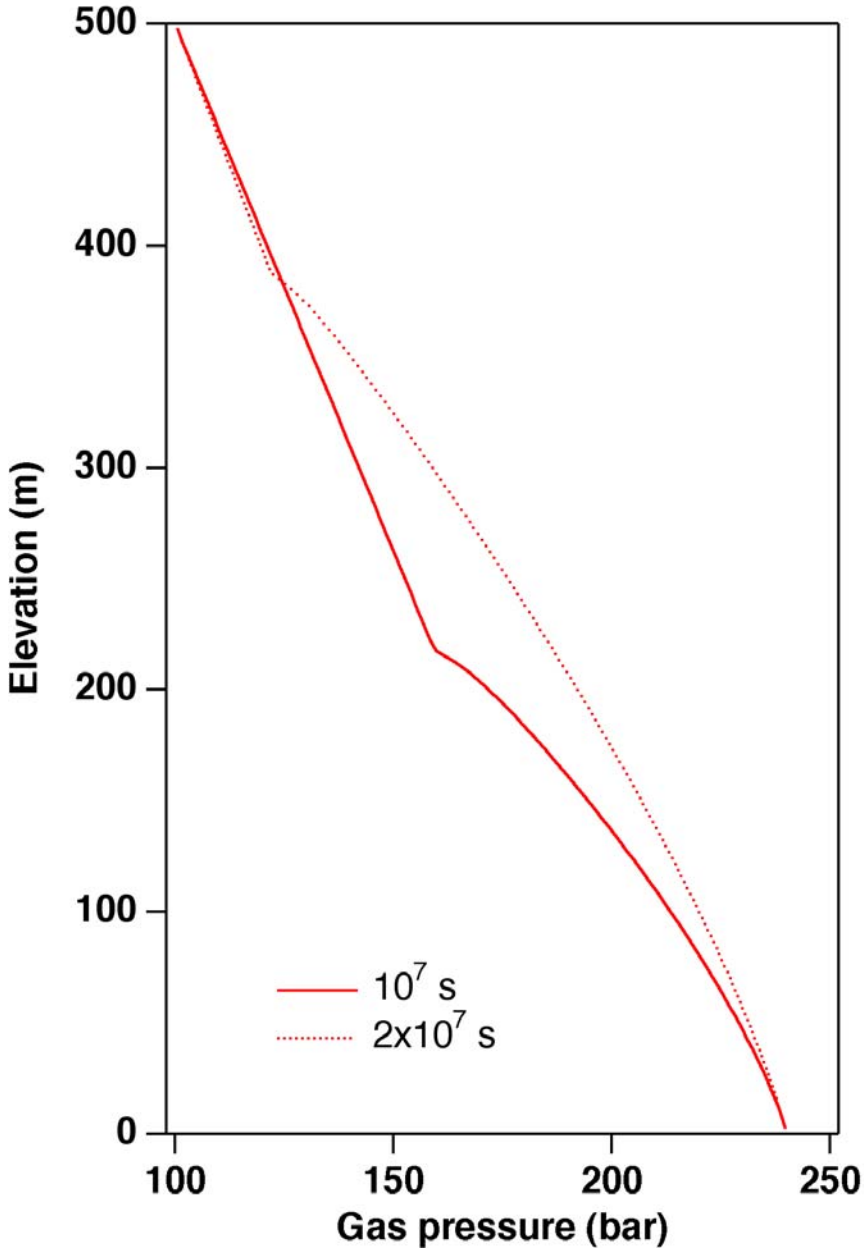

Figure 3.5 Pressure profiles at times of 10^7 and $2x10^7$ seconds.

CO2 gas entering from the block below is dissolved in the aqueous phase. The CO2 volume entering the block in effect disappears from the system, so that pressures decline. When the CO2 solubility limit is exceeded and a free gas phase forms this is accompanied by very rapid pressurization. Eventually gas saturation in the monitoring block increases to the point where gas phase becomes mobile, and is able to flow out to the next block above. This outflow is accompanied by rapid depressurization, which causes further increases in gas saturation due to expansion,

enhancing gas mobility and accelerating outflow. From these considerations it is apparent that pressures are subject to severe fluctuations that are caused by space discretization effects. Simulated pressures have physical significance only in a time-averaged sense.

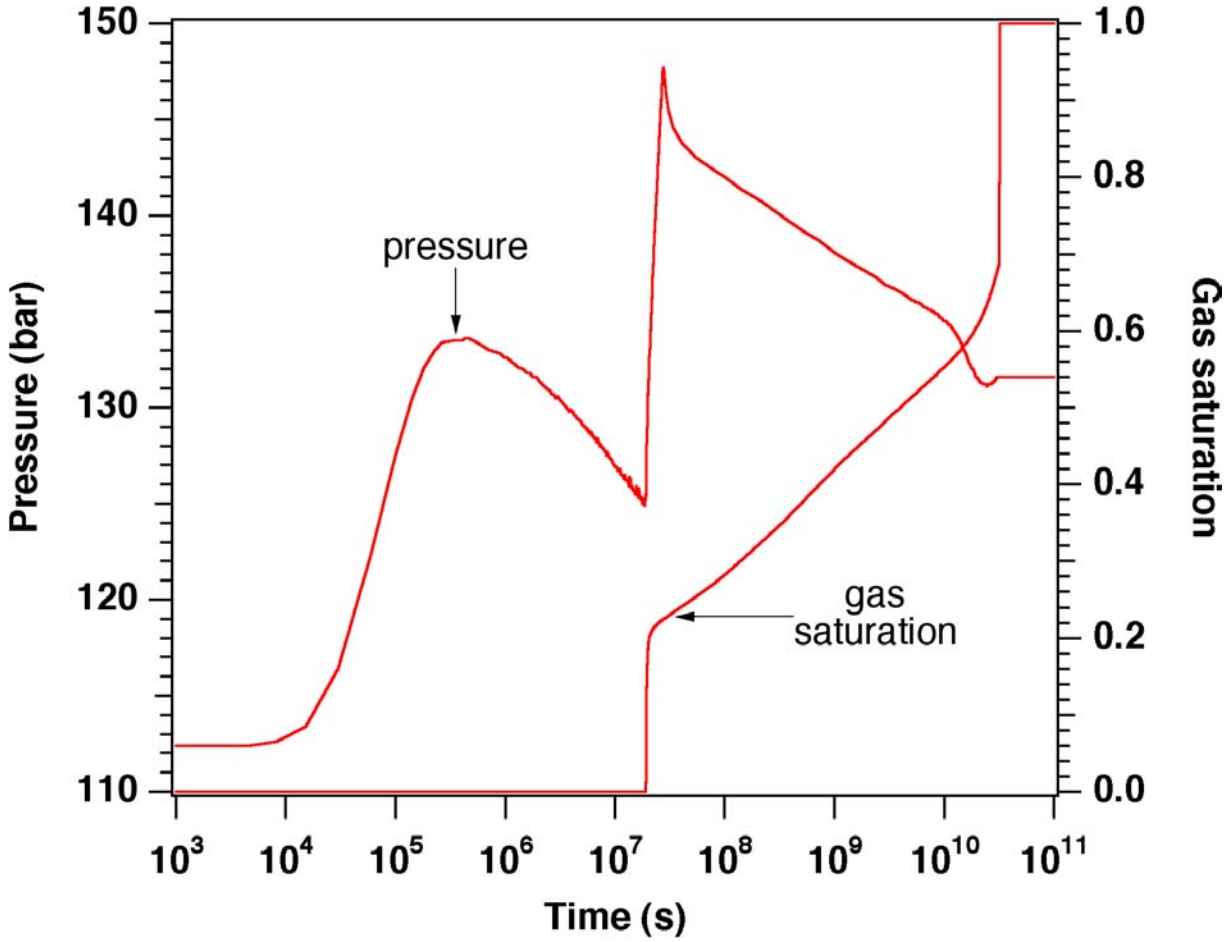

Figure 3.6 Transient evolution of pressures and gas saturations at a monitoring grid block, 372.5 m up the fault.

3.5 Non-isothermal Variation

To examine temperature effects associated with CO2 injection a non-isothermal version of the problem was simulated. This uses the same input file as shown in Fig. 3.2, except that in data block MULTI we specified to solve NEQ=4 equations, including the three mass balances for water, salt, and CO2, and a heat balance. (TOUGH2/ECO2 always solves a salt mass balance even if all salt concentrations are specified as zero.) For the thermal parameters we use generic values, including rock specific heat of 920 J/kg ˚C, and formation thermal conductivity of 2.51 W/m ˚C. CO2 is injected at conditions of P = 240 bar, T = 45 ˚C; thermal conductivity of the injection grid

block was set to zero, to avoid spurious heat conduction from that block into the fault system. Fig. 3.7 compares results for isothermal and non-isothermal calculations in which the Poynting correction for CO2 solubility was neglected. It is seen that gas saturation profiles at 10^7 seconds for the non-isothermal run are virtually identical to those obtained for the isothermal version.

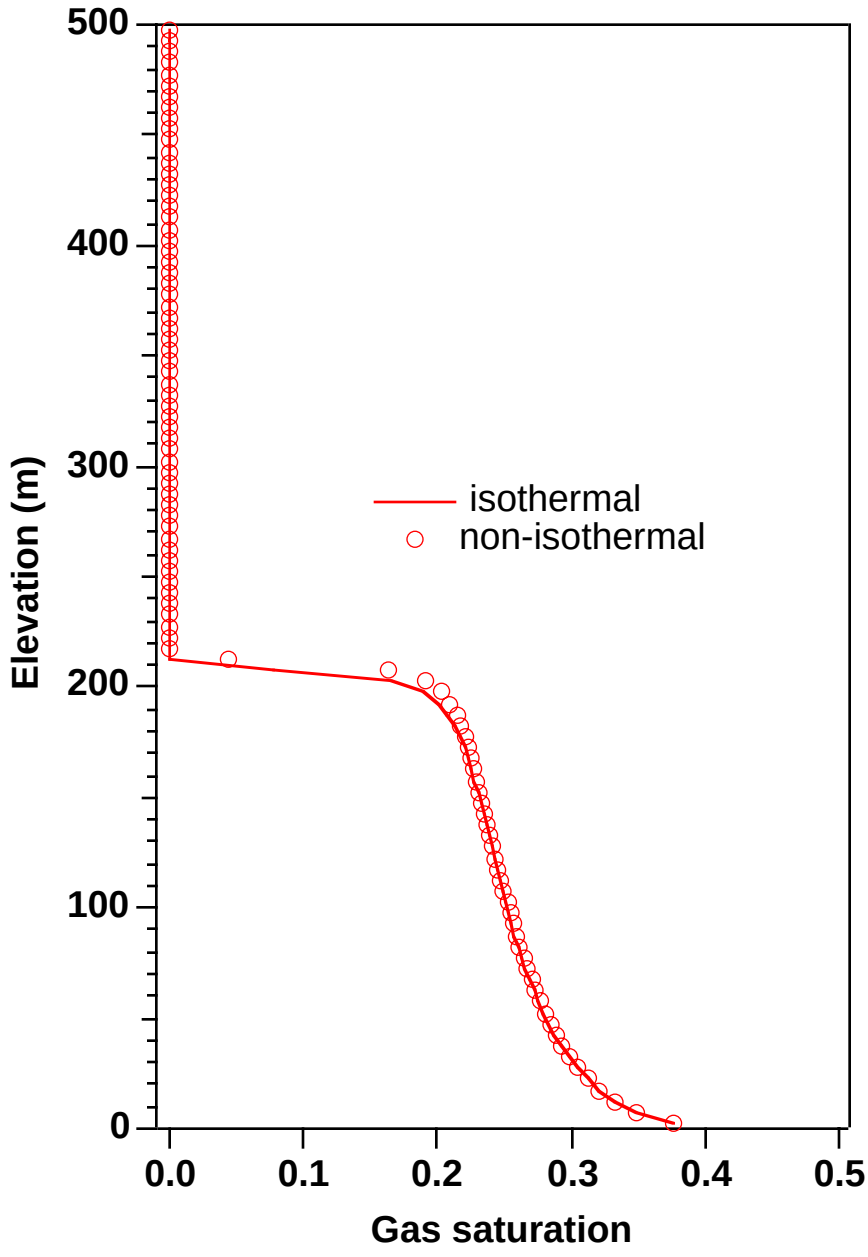

Figure 3.7 Gas saturation profiles at 10^7 seconds for isothermal and non-isothermal conditions.

Fig. 3.8 shows simulated temperature profiles at a time of 10^7 seconds, as well as for the steady single-phase gas flow conditions that are eventually reached at large simulation time. At 10^7

seconds, temperatures in most of the two-phase zone are increased by approximately 3 ˚C relative to the initial T = 45 ˚C, reflecting heat-of-dissolution effects as a portion of the CO2 is dissolved in the aqueous phase. At early times the temperature increase from heat-of-dissolution effects starts right at the injection boundary, but at later times some cooling occurs due to decompression of CO2 as it is flowing upwards. Fig. 3.9 presents the dependence of the specific enthalpy of CO2 on

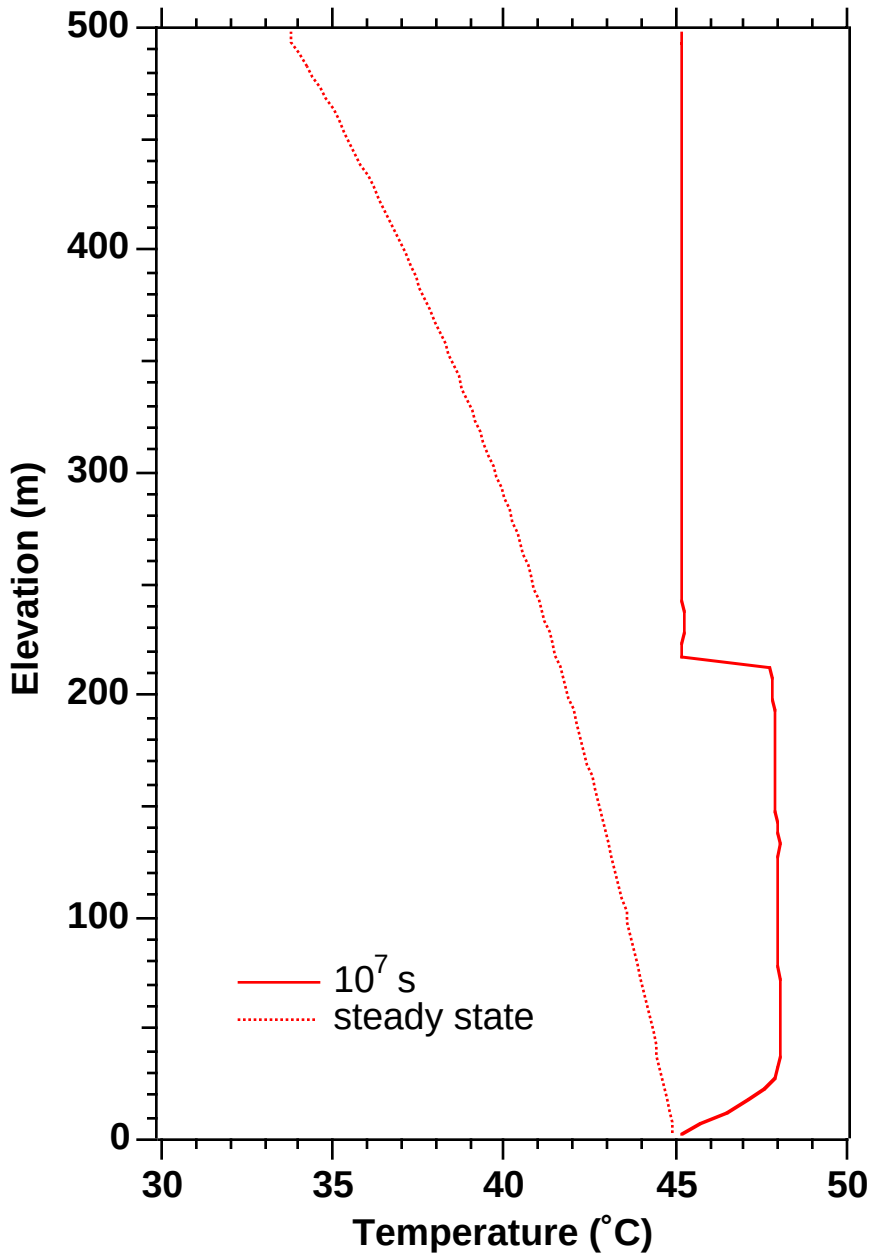

Figure 3.8 Temperature profiles for a non-isothermal version of the problem at 10^7 seconds, and at the eventual steady state conditions.

temperature and pressure, calculated from the correlations of Altunin (1975) used in our simulation. It is seen that adiabatic (isenthalpic) decompression of CO2 will result in a temperature decline, which explains the nature of the temperature profile obtained for the single-phase gas flow conditions at late time (Fig. 3.8).

Small temperature increases of approximately 0.2 ˚C are seen at 10^7 seconds ahead of the two-phase front. These are caused by compression effects in the aqueous phase.

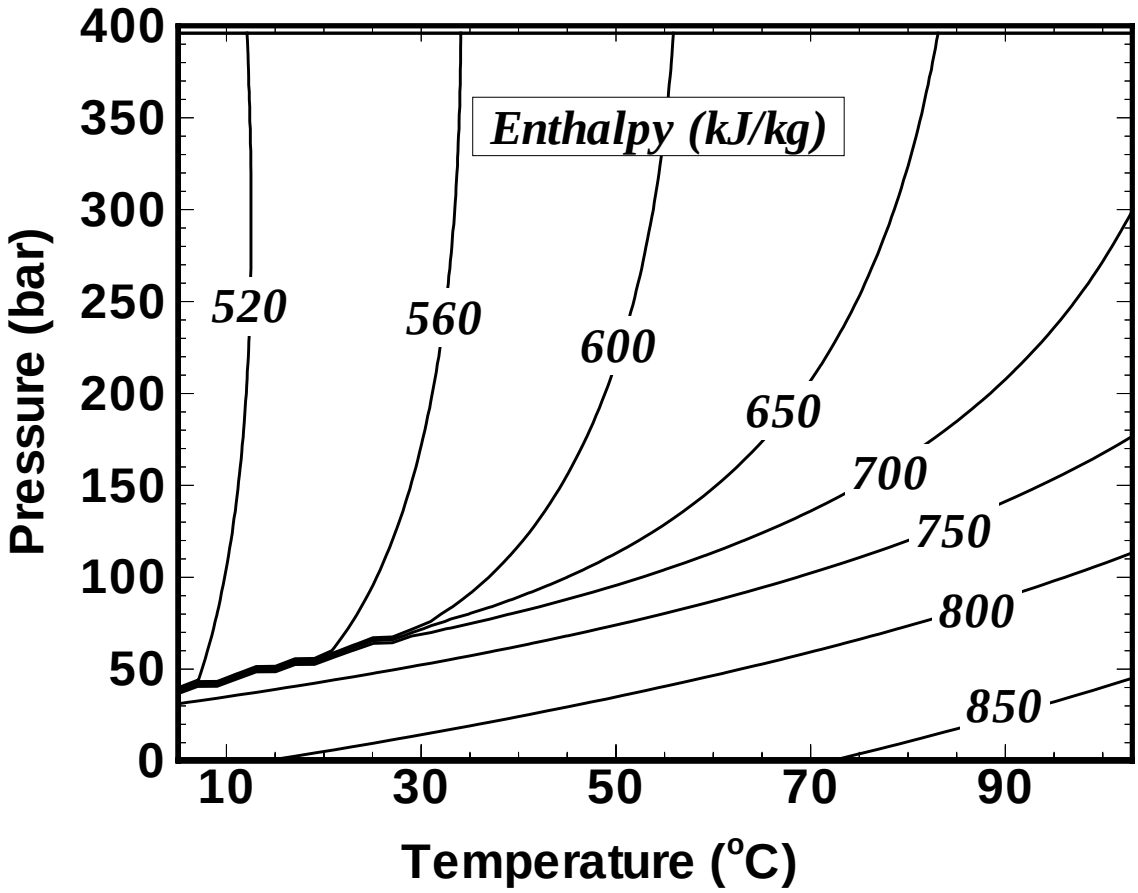

Figure 3.9 Enthalpy of pure CO2 as function of temperature and pressure, as calculated from the correlations of Altunin (1975).

4. Problem 7. CO2 Injection into a 2-D Layered Brine Formation

The only industrial-scale CO2 disposal project currently in operation is at the Sleipner Vest field in the Norwegian sector of the North Sea, where approximately 10^6 tonnes of CO2 per year are injected through a horizontal well into sands of the Utsira formation. Time-lapse seismic surveys have shown that CO2 migration at Sleipner is dominated by buoyancy effects and is strongly affected by shale interbeds of low permeability (Lindeberg et a., 2001). Test problem 7 was patterned after conditions at Sleipner and was designed to investigate CO2 migration in a heterogeneous sand-shale sequence. A 2-D vertical section was modeled (Fig. C.1, Appendix C), with problem specifications given in Appendix C.

This problem was simulated with the TOUGH2/ECO2 code, using fluid property descriptions as summarized in section 3, except that here we did not include a Poynting correction for CO2 solubility in the aqueous phase. Consequently, CO2 solubility in the aqueous phase is overestimated by as much as 1.5 percentage points which, however, has only a small impact on simulated system behavior. The problem was run in several segments to first obtain the initial and boundary conditions, and then inject CO2 according to specifications. All runs were performed in isothermal mode at a temperature of 37 ˚C. Both a fresh water case and a case with 3.2 wt.-% salinity (NaCl) were run.

The grid should be designed in such a way as to obtain “adequate” spatial resolution in regions where significant gradients occur, i.e., near the injection well, and near the shale layers (Fig. C.1). Also, simulation results are desired along prescribed horizontal and vertical profiles, and the gridding needs to accommodate these requirements. The grid is generated with the MESHMAKER facility of TOUGH2 as a horizontal (x-y) grid and is then rotated by 90 degrees around the x-axis to obtain a vertical section. Subroutine GXYZ was modified to automatically assign “sand” and “shale” domain identifiers to grid blocks at the appropriate elevations. Gridding in the x-direction starts with 1 m increments at the well, and becomes coarser at increasing distance (Table 4.1). 28 grid blocks are used to get out to a distance of 6,000 m, followed by a small grid increment of 10^{-3} m to serve as boundary blocks to maintain a hydrostatic pressure profile. Gridding in the y-direction also uses a 1 m increment at the well, with coarser gridding below and above. The shale layers are represented as single grid layers of 3 m height, with 3 m gridding also in the sands above and below. The thickness of the grid is 1 m. Overall the gridding is considered rather coarse, meeting minimum requirements for spatial resolution at the well and at the shale layers.

Table 4.1 Grid increments (29 blocks in x from left to right; 34 blocks in y from bottom to top).

```
MESHMAKER1----*----2----*----3----*----4----*----5----*----6----*----7----*----8
XYZ
       90.
NX      29
        1.        1.        2.        4.        4.        8.       15.       20.
       30.       40.       50.       50.      100.      150.       50.      150.
      300.       50.      475.      500.      500.      500.      500.      500.
      500.      500.      500.      500.     1.e-3
NY      34
        7.        6.        6.       2.5        1.       2.5        6.       12.
        6.        3.        3.        3.        6.       12.        6.        3.
        3.        3.        6.       12.        6.        3.        3.        3.
        6.       12.        6.        3.        3.        3.        6.       12.
        6.        3.
NZ       1       1.0
```

4.1 Thermophysical Properties

Formation waters have a CO2 partial pressure of 0.5 bars, and are either fresh water or have a salinity of 3.2 % by weight. Salinity specifications can be directly input into TOUGH2, as salt mass fraction is one of the primary variables. CO2 concentrations in TOUGH2/ECO2 are specified in terms of mass fractions as well, and brief trial-and-error runs were made to obtain the CO2 mass fractions that would correspond to a partial pressure of 0.5 bar, as stipulated in the problem specifications. The appropriate CO2 mass fractions were found to be 5.3009×10^{-4} (fresh water), 4.5998×10^{-4} (3.2 weight-% brine), and 1.14795×10^{-4} (saturated brine), reflecting the "salting out" effect of decreasing CO2 solubility with increasing salinity. NaCl mass fraction in saturated brine is 26.63 weight-%.

Representative fluid properties as used in TOUGH2/ECO2 are given in Tables 4.2 and 4.3 for a temperature of 37 ˚C at different salinities for a range of pressures. No allowance is presently made for dependence of brine density and viscosity on dissolved CO2.

Table 4.2. PVT properties at a temperature of 37 ˚C for different salinities (no CO2).

(a) density, kg/m^3

pressure (bars)	fresh water	3.2 wt.-% brine	saturated brine
90	996.68	1017.83	1196.26
100	997.05	1018.19	1196.71
120	997.79	1018.92	1197.61
140	998.54	1019.65	1198.51
160	999.28	1020.38	1199.41
180	1000.02	1021.11	1200.31

(b) viscosity, 10^{-4} Pa-s

pressure (bars)	fresh water	3.2 wt.-% brine	saturated brine
90	6.9208	7.3201	14.055
100	6.9214	7.3207	14.056
120	6.9225	7.3219	14.058
140	6.9237	7.3232	14.061
160	6.9251	7.3246	14.063
180	6.9265	7.3261	14.066

Table 4.3. PVT properties at a temperature of 37 ˚C for two-phase fluid mixtures of water, CO2, and NaCl.

(a) fresh water (no salinity)

pressure (bars)	aq. density (kg/m^3)	gas density (kg/m^3)	aq. viscosity (10^{-4} Pa s)	gas viscosity (10^{-5} Pa s)	CO2 mass fraction (aq.; 10^{-2})	H2O mass fraction (gas; 10^{-5})
90	996.68	606.61	6.9208	4.5731	5.8600	7.2422
100	997.05	684.06	6.9214	5.4613	6.2100	6.4221
120	997.79	749.33	6.9225	6.3711	6.8100	5.8627
140	998.54	787.46	6.9237	6.9830	7.3000	5.5789
160	999.28	815.36	6.9251	7.4752	7.6900	5.3880
180	1000.02	837.59	6.9265	7.8982	8.0300	5.2449

(b) 3.2 weight-% salinity

pressure (bars)	aq. density (kg/m^3)	gas density (kg/m^3)	aq. viscosity (10^{-4} Pa s)	gas viscosity (10^{-5} Pa s)	CO2 mass fraction (aq.; 10^{-2})	H2O mass fraction (gas; 10^{-5})
90	1017.83	606.62	7.3201	4.5733	5.1071	7.0995
100	1018.19	684.07	7.3207	5.4614	5.4147	6.2957
120	1018.92	749.33	7.3219	6.3711	5.9388	5.7474
140	1019.65	787.46	7.3232	6.9830	6.3642	5.4691
160	1020.38	815.36	7.3246	7.4753	6.7134	5.2820
180	1021.11	837.6	7.3261	7.8982	7.0043	5.1418

4.2 Gravity Equilibration

Initial conditions are generated in stages. A first simulation run involves just the column of boundary grid blocks beyond x = 6,000 m. Thermodynamic properties are specified as P = 110 bars, T = 37 ˚C, salinity X_s = 0.032, CO2 mass fraction X_{CO2} = 4.5998x10^{-4}. Pressure is held constant at P = 110 bar at the elevation of the injection node (22 m) and the system is run to gravity equilibrium. To facilitate reaching an accurate equilibrium state, the shale layers are given the same

absolute permeability as the sand layers for this simulation. Gravity equilibrium using a tight convergence tolerance of 10^{-8} is attained in seven time steps for both fresh water and 3.2 wt.-% salinity cases, corresponding to a simulation time of 3.25×10^{9} s. Maximum pore velocities in the equilibrium state are below 10^{-17} m/s. The pressure profiles at gravity equilibrium are given in Fig. 4.1, showing only small differences between the fresh water and 3.2 % salinity cases. A second run with the full two-dimensional grid is then performed, using the same initialization as for the 1-D gravity equilibration just described, and maintaining the 1-D gravity equilibrium as boundary conditions at the right hand side. For this calculation we again specify the same absolute permeability for shale as for sand. Gravity equilibration in the 2-D grid takes 14 time steps for the fresh water case, and 12 time steps for 3.2 wt.-% salinity, for simulation times of 1.14×10^{10} s and 2.93×10^{9} s, respectively.

4.3 CO2 Injection

The TOUGH2 input file for CO2 injection into brine with 3.2 wt.-% salinity at a constant prescribed rate of 0.1585 kg/s is shown in Fig. 4.2. This input file specifies a total simulation time of 2.592×10^{6} s (30 days), because CO2 mass balances are desired at this time. Continuation runs are then performed to reach times of one year (3.15576×10^{7} s) and two years (6.31152×10^{7} s). The runs with and without salinity proceed in very similar fashion, and both require 587 time steps to reach the final simulation time of two years. Time steps gradually increase during the course of the simulation, as can be seen from the negative curvature of the time step vs. time curve in Fig. 4.3. Gas saturation at the wellblock quickly reaches a quasi-steady value of approximately 53 % (Fig. 4.3). Fluid salinity at the wellblock keeps increasing over time as water is slowly being removed by evaporation into the CO2 stream (Fig. 4.4). CO2 mass fraction in the aqueous phase slowly decreases, as CO2 solubility declines with increasing salinity.

Figs. 4.5 and 4.6 show contour plots of gas saturation and CO2 mass fraction dissolved in the aqueous phase after two years of CO2 injection. Highest gas saturations of approximately 60 % occur beneath the shale layers at elevations of 52, 85, and 118 m. Gas is just beginning to reach the top shale layer at an elevation of 151 m. CO2 mass fraction dissolved in the aqueous phase after two years is in the range of 5 - 6 % throughout most of the two-phase zone, with smaller but significant aqueous CO2 concentrations occurring beyond the two-phase region.

Gas saturations along vertical profiles at different distances from the left boundary after two years are shown in Fig. 4.7. Buoyancy effects are evident from the large gas saturations beneath the shales, and from the increase in elevation of the lower boundary of the two-phase zone with increasing distance from the injection well. In the time period from one to two years, gas saturations

at 200 m distance increase most strongly beneath and above the third shale layer at 118 m elevation (Fig. 4.8). Gas saturation profiles for the simulations with and without salinity are almost identical (Fig. 4.9), the most significant difference being the slightly larger gas saturation beneath the top shale (elevation 151 m) for the saline case. This can be understood from the reduced CO2 solubility under saline conditions, which places a slightly larger fraction of total CO2 into the gas phase, see Table 4.4.

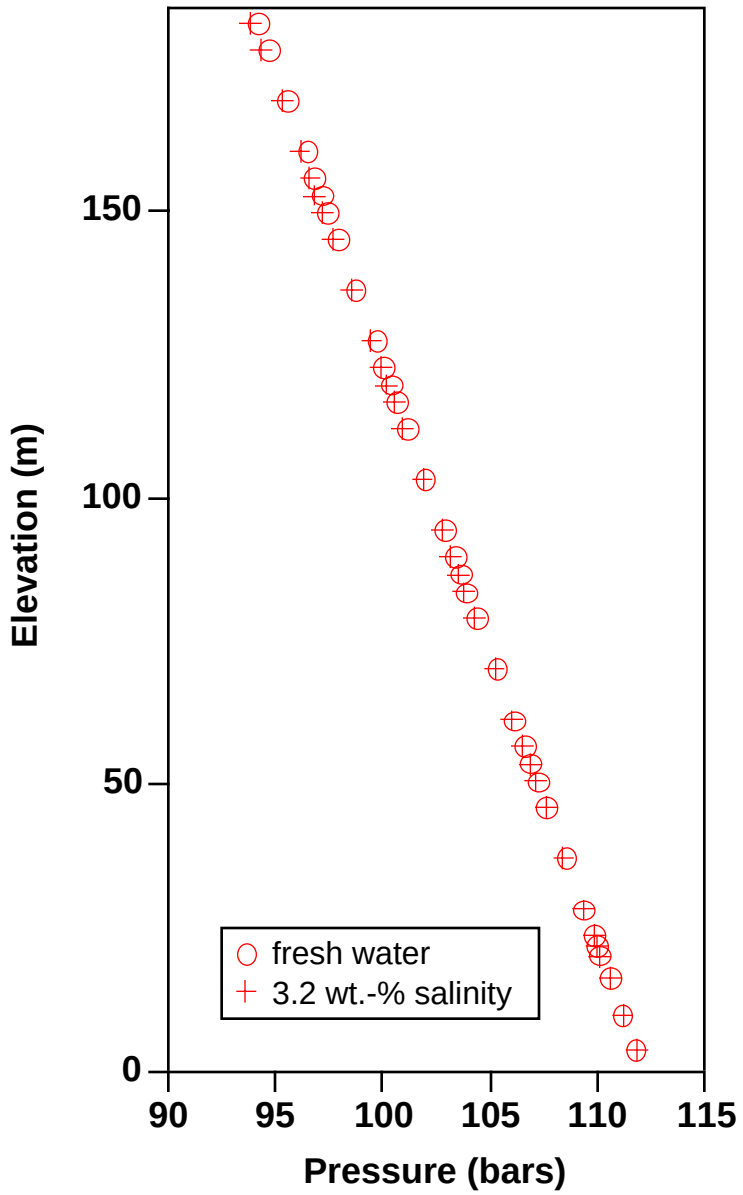

Figure 4.1 Hydrostatic pressure profile prior to CO2 injection.

```
*rtp7* ... test problem # 7: CO2 in layered formation
ROCKS----1----*----2----*----3----*----4----*----5----*----6----*----7----*----8
sand     2  2600.e00       .35    3.e-12    3.e-12    3.e-12      2.51      920.
   0.0e-10
    7           0.40      0.20        1.      0.05
    7           0.40      0.20   2.79e-4      1.e7      .999
shale    2  2600.e00     .1025   10.e-15   10.e-15   10.e-15      2.51      920.
   0.0e-10
    7           0.40      0.20        1.      0.05
    7           0.40      0.20   1.61e-5      1.e7      .999

MULTI----1----*----2----*----3----*----4----*----5----*----6----*----7----*----8
    3    3    3    6
SELEC....2....3....4....5....6....7....8....9...10...11...12...13...14...15...16
    1                                           0    0    0    2    0    0    2
        .8   .8
     ..... IE(16) = 2 chooses CO2, = 3 is for methane.
START----1----*----2----*----3----*----4----*----5----*----6----*----7----*----8
----*----1 MOP: 123456789*123456789*1234 ---*----5----*----6----*----7----*----8
PARAM----1----*----2----*----3----*----4----*----5----*----6----*----7----*----8
   1 600    99991000 00000000  4    3
             2.592e6       -1.                          -9.81
      1.e2
     1.E-5     1.E00
              110.e5              3.2e-2          .45998E-03                 37.
SOLVR----1----*----2----*----3----*----4----*----5----*----6----*----7----*----8
5  Z1   O0    8.0e-1    1.0e-7
GENER----1----*----2----*----3----*----4----*----5----*----6----*----7----*----8
A15 1inj 1                   1     COM3      .1585

TIMES----1----*----2----*----3----*----4----*----5----*----6----*----7----*----8
    3
   2.592e6 31.5576e6 63.1152e6
FOFT ----1----*----2----*----3----*----4----*----5----*----6----*----7----*----8
A15 1          sand  .1000E+01 .2000E+01           .5000E+00 .2200E+02-.5000E+00
A1A 1          sand  .3000E+01 .6000E+01           .5000E+00 .5050E+02-.5000E+00
A1G 1          sand  .3000E+01 .6000E+01           .5000E+00 .8350E+02-.5000E+00
A1U 1          sand  .3000E+01 .6000E+01           .5000E+00 .1555E+03-.5000E+00
A1A13          sand  .3000E+03 .6000E+03           .3000E+03 .5050E+02-.5000E+00

COFT ----1----*----2----*----3----*----4----*----5----*----6----*----7----*----8
A1B 1A1C 1                   2 .1500E+01 .1500E+01 .1000E+01 .1000E+01

ENDCY----1----*----2----*----3----*----4----*----5----*----6----*----7----*----8
```

Figure 4.2 TOUGH2 input file for CO2 injection into layered brine formation.

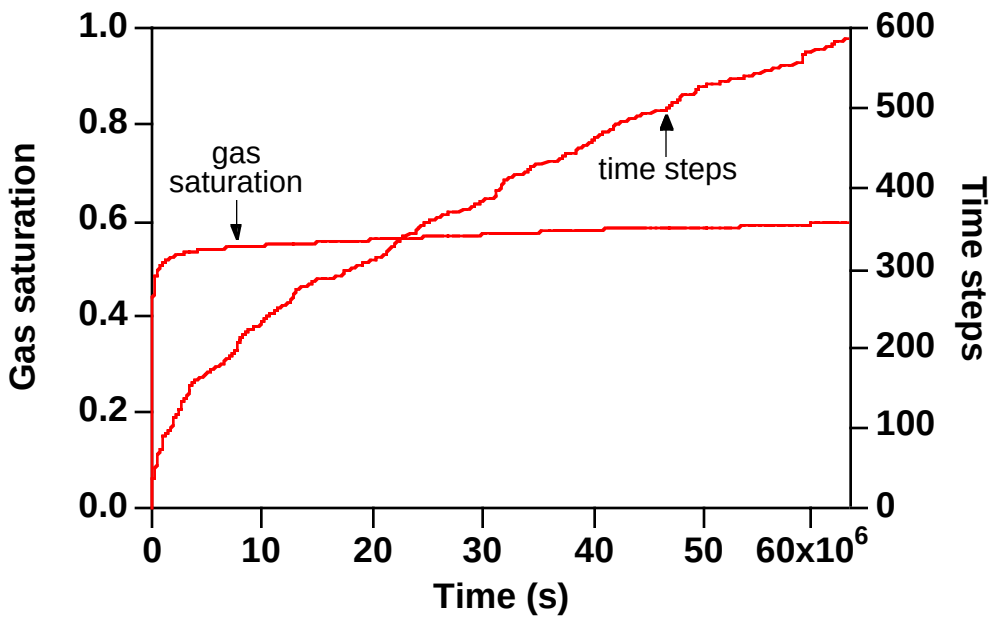

Figure 4.3 Time stepping and gas saturation vs. time at the wellblock for the case with 3.2 wt.-% salinity.

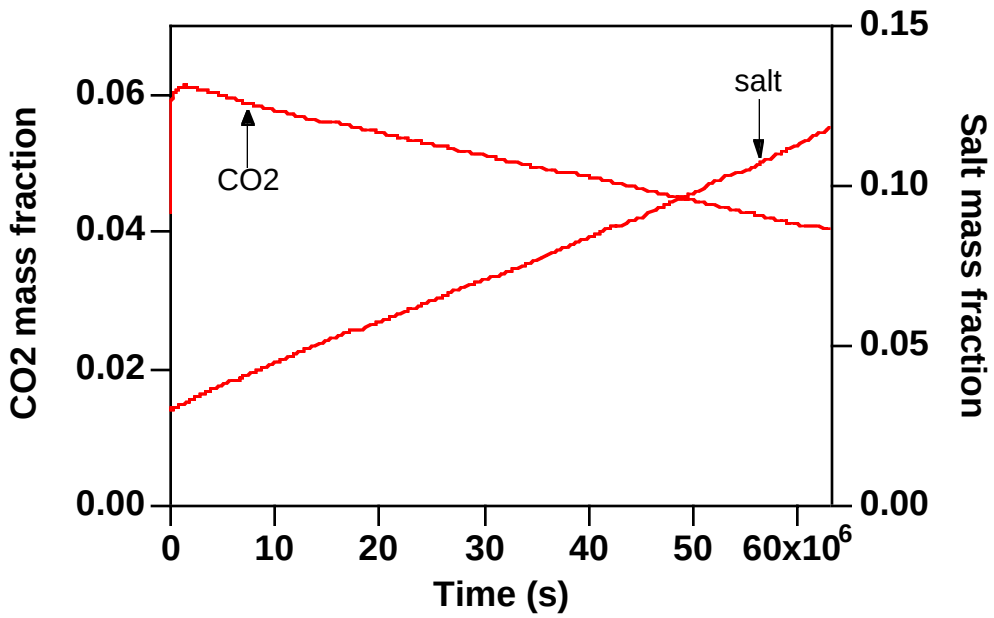

Figure 4.4 CO2 and salt mass fractions in the aqueous phase at the wellblock for the case with 3.2 wt.-% salinity.

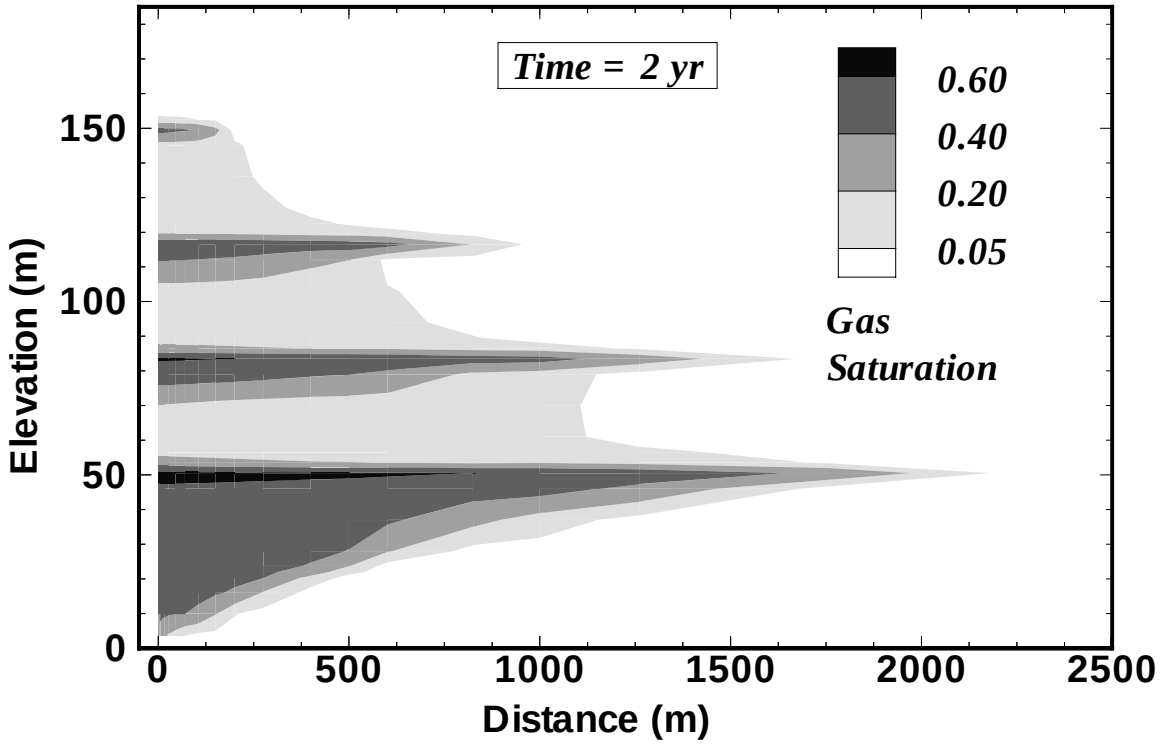

Figure 4.5 Gas saturation after 2 years of CO2 injection for the case with 3.2 wt.-% salinity.

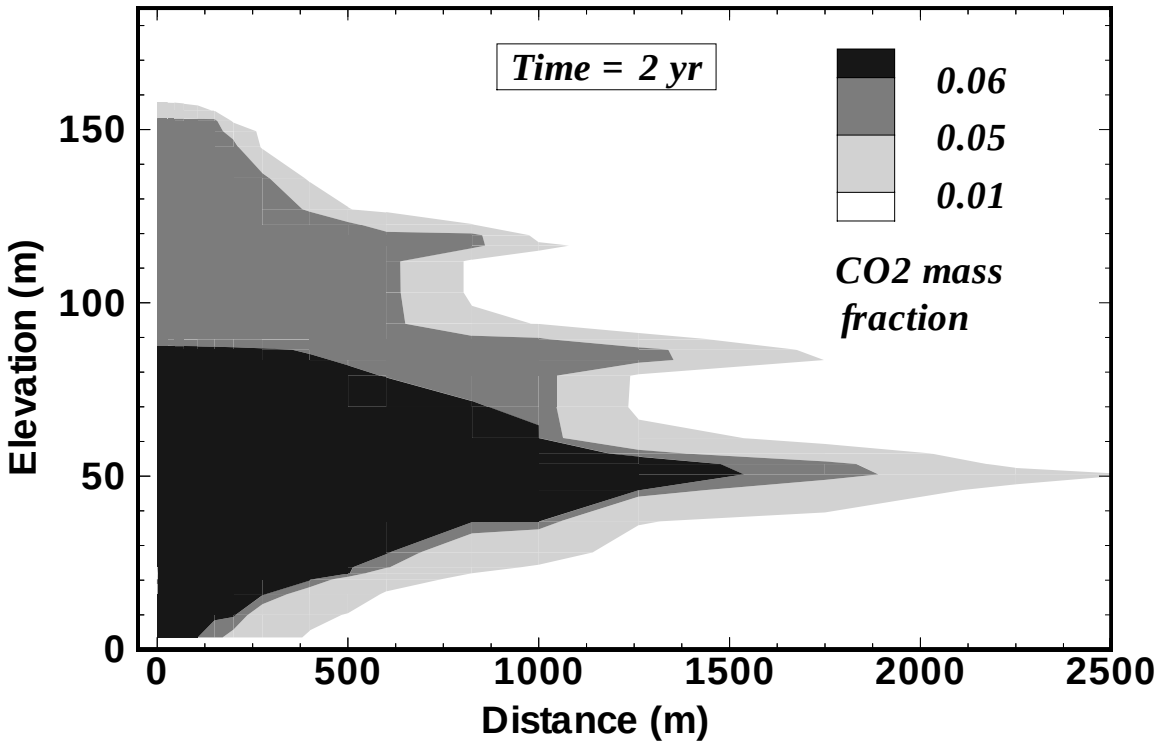

Figure 4.6 CO2 mass fraction dissolved in the aqueous phase after 2 years of CO2 injection for the case with 3.2 wt.-% salinity.

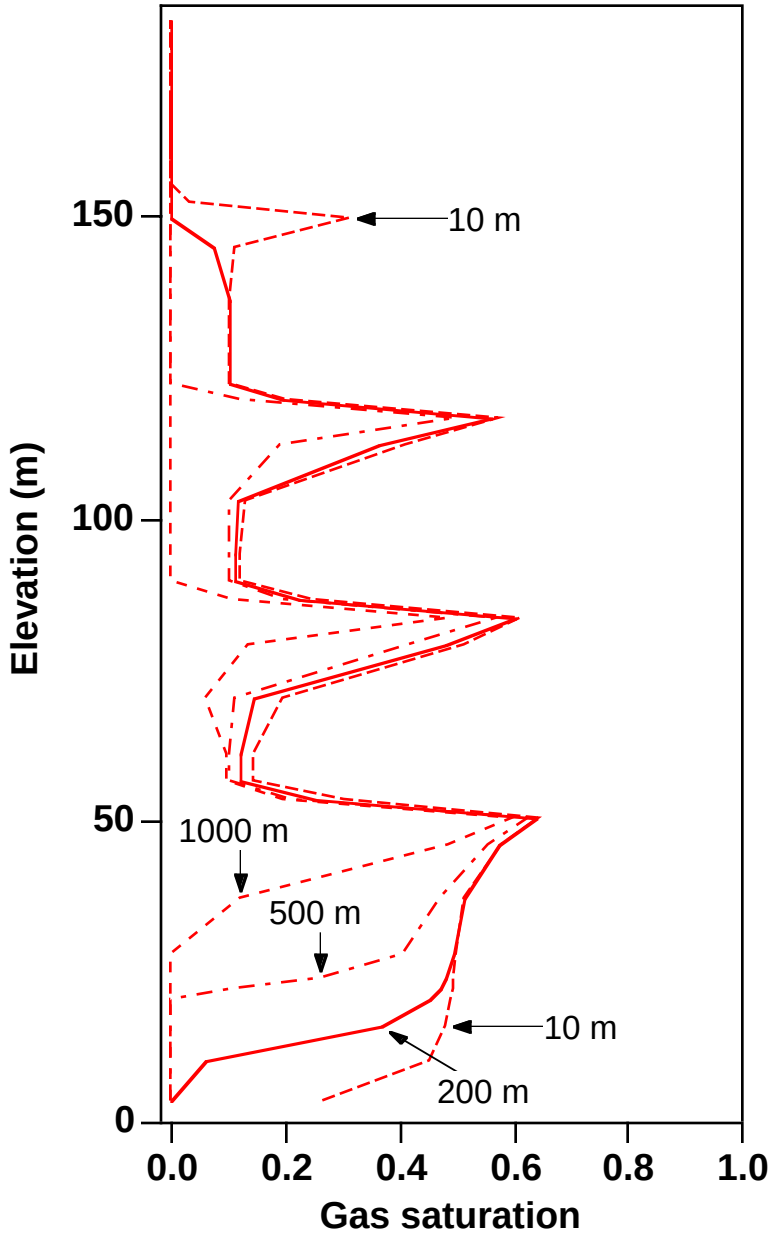

Figure 4.7 Vertical profiles of gas saturation after two years at different distances from the left boundary for the case with 3.2 wt.-% salinity.

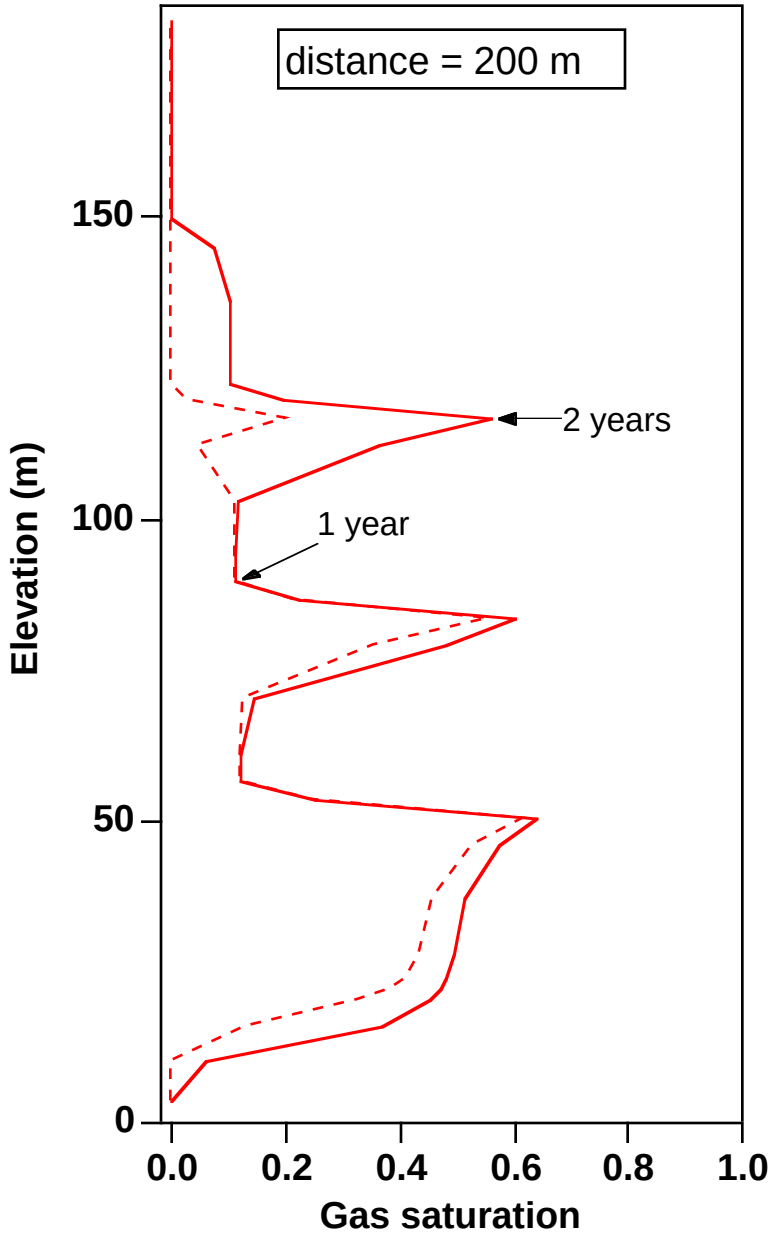

Figure 4.8 Vertical profiles of gas saturation at 200 m distance from the left boundary for the case with 3.2 wt.-% salinity.

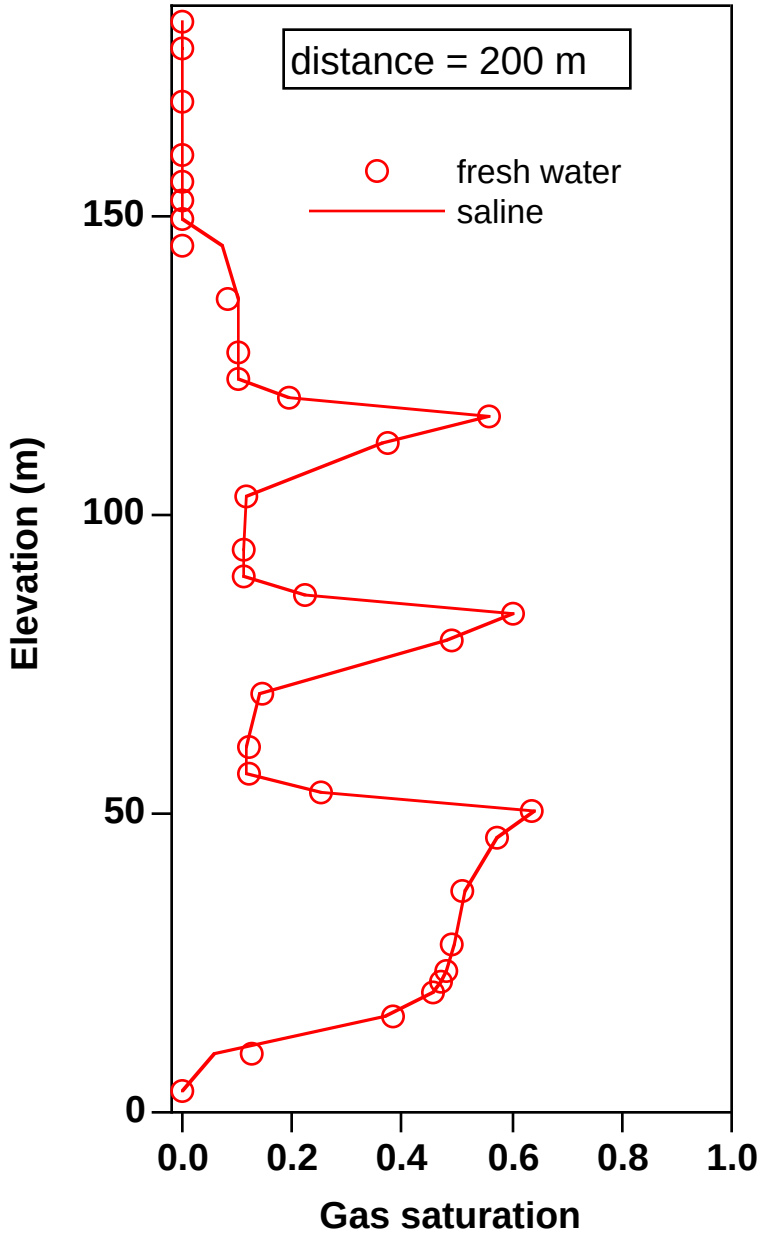

Figure 4.9 Vertical profiles of gas saturation at 200 m distance from the left boundary after 2 years.

Table 4.4 CO2 mass balances (in units of 10^6 kg) for injection into fresh water and saline systems.

	t = 0		30 days		1 year		2 years	
	fresh	saline	fresh	saline	fresh	saline	fresh	saline
total CO2	0.2042	0.1810	0.6149	0.5916	5.203	5.180	10.20	10.18
CO2 injected	0.0000		0.4108		5.002		10.00	
CO2 (aq.)	0.2042	0.1810	0.3184	0.2876	1.360	1.274	2.525	2.330
CO2 (gas)	0.0000	0.0000	0.2965	0.3040	3.843	3.906	7.677	7.849
fraction of CO2 in aq. phase	1.000	1.000	0.5178	0.4861	0.2614	0.2460	0.2475	0.2289

5. Concluding Remarks

This study has considered three numerical simulation problems for displacement of water by CO2 that were posed as part of an intercomparison study of numerical simulation codes. The problems considered are prototypical for, respectively, CO2 injection from a vertical well (Problem 3), leakage of CO2 from a storage reservoir (Problem 4), and disposal of CO2 into a layered heterogeneous formation from a horizontal well (Problem 7). LBNL's general purpose TOUGH2 reservoir simulator was used in conjunction with special fluid property modules developed for multiphase mixtures of water, CO2 and salt (NaCl) for the temperature and pressure conditions of interest in geologic disposal of CO2. Issues addressed in the simulations include thermophysical properties of fluids, phase partitioning between aqueous and CO2-rich (gas-like) phases, immiscible displacement of water by CO2, interplay of viscous, gravitational, and capillary forces, and role of heterogeneities. Detailed results for simulated systems behavior are given along with data for fluid properties, to provide benchmarks against which other simulation codes may be tested.

Acknowledgement

We thank Christine Doughty and André Unger for a review of the manuscript. The specifications for Problem 7 were developed by Carl Steefel. This work was supported by the U.S. Department of Energy through the Office of Basic Energy Sciences and through the National Energy Technology Laboratory (NETL) under Contract No. DE-AC03-76SF00098.

References

Altunin, V.V. *Thermophysical Properties of Carbon Dioxide,* Publishing House of Standards, 551 pp., Moscow, 1975 (in Russian).

Battistelli, A., C. Calore and K. Pruess. The Simulator TOUGH2/EWASG for Modeling Geothermal Reservoirs with Brines and Non-Condensible Gas, *Geothermics,* Vol. 26, No. 4, pp. 437 - 464, 1997.

Chou I.M. Phase Relations in the System NaCl-KCl-H_2O. III: Solubilities of Halites in Vapor-Saturated Liquids above 445 ˚C and Redetermination of Phase Equilibrium Properties of the System NaCl-H_2O. *Geochim Cosmochim Acta,* Vol. 51, pp. 1965 - 1975, 1987.

Doughty, C. and K. Pruess. A Similarity Solution for Two-Phase Water, Air and Heat Flow Near a Linear Heat Source in a Porous Medium, *J. of Geophys. Res.*, Vol. 97 (B2), pp. 1821 - 1838, 1992.

García, J. Density of Aqueous Solutions of CO2, Lawrence Berkeley National Laboratory Report LBNL-49023, Berkeley, CA, 2001.

Haas, J.L. Jr. Physical Properties of the Coexisting Phases and Thermochemical Properties of the H2O Component in Boiling NaCl solutions, USGS Bulletin 1421-A, Washington, DC, 73 pp., 1976.

Hitchon, B. (ed.). *Aquifer Disposal of Carbon Dioxide,* Geoscience Publishing, Ltd., Sherwood Park, Alberta, Canada, 1996.

International Formulation Committee. A Formulation of the Thermodynamic Properties of Ordinary Water Substance, IFC Secretariat, Düsseldorf, Germany, 1967.

Lindeberg, E., P. Zweigel, P. Bergmo, A. Ghaderi, and A. Lothe. Prediction of CO2 Distribution Pattern Improved by Geologic and Reservoir Simulation and Verified by Time Lapse Seismic, in: D. Williams et al. (eds.), *Proceedings,* Fifth International Conference on Greenhouse Gas Control Technologies, pp. 372 - 377, CSIRO Publ., Collingwood, VIC, Australia, 2001.

Oldenburg, C.M., D. H.-S. Law, Y. Le Gallo, and S.P. White. Mixing of CO2 and CH4 in Gas Reservoirs: Code Comparison Studies, paper F1-1, presented at Sixth International Conference on Greenhouse Gas Technologies (GHGT-6), Kyoto, Japan, October 1-4, 2002.

O'Sullivan, M.J. A Similarity Method for Geothermal Well Test Analysis, *Water Resour. Res.*, Vol. 17, No. 2, pp. 390 – 398, 1981.

Pape, H., C. Clauser and J. Iffland. Permeability Prediction Based on Fractal Pore-Space Geometry, *Geophysics,* Vol. 64, No. 5, pp. 1447 - 1460, 1999.

Phillips, S.L., A. Igbene, J.A. Fair, H. Ozbek and M. Tavana. A Technical Databook for Geothermal Energy Utilization, Lawrence Berkeley National Laboratory Report LBL-12810, Berkeley, CA, 46 pp., 1981.

Prausnitz, J. M., R. N. Lichtenthaler, and E. G. de Azevedo. *Molecular Thermodynamics of Fluid-Phase Equilibria,* Prentice-Hall Inc., Englewood Cliffs, N. J., 1986.

Pruess, K., C. Oldenburg and G. Moridis. TOUGH2 User's Guide, Version 2.0, Lawrence Berkeley National Laboratory Report LBNL-43134, Berkeley, CA, November 1999.

Pruess, K., C.F. Tsang, D. H.-S. Law and C.M. Oldenburg. Intercomparison of Simulation Models for CO2 Disposal in Underground Storage Reservoirs, Lawrence Berkeley National Laboratory Report LBNL-47353, October 2000.

Pruess, K. and J. García. Multiphase Flow Dynamics During CO2 Injection into Saline Aquifers, *Environmental Geology*, Vol. 42, pp. 282 - 295, 2002.

Pruess, K., A. Bielinski, J. Ennis-King, R. Fabriol, Y. Le Gallo, J. García, K. Jessen, T. Kovscek, D. H.-S. Law, P. Lichtner, C. Oldenburg, R. Pawar, J. Rutqvist, C. Steefel, B. Travis, C.F. Tsang, S. White, T. Xu. Code Intercomparison Builds Confidence in Numerical Models for Geologic Disposal of CO2, paper F1-4, presented at Sixth International Conference on Greenhouse Gas Technologies (GHGT-6), Kyoto, Japan, October 1-4, 2002a. (LBNL-51200)

Pruess, K., J. García, T. Kovscek, C. Oldenburg, J. Rutqvist, C. Steefel and T. Xu. Intercomparison of Numerical Simulation Codes for Geologic Disposal of CO2, Lawrence Berkeley National Laboratory Report LBNL-51813, Berkeley, CA 94720, December 2002b.

Spycher, N., K. Pruess and J. Ennis-King. CO_2-H_2O Mixtures in the Geological Sequestration of CO_2. I. Assessment and Calculation of Mutual Solubilities from 12 to 100 °C and up to 600 bar, submitted to *Geochim. Cosmochim. Acta*, July 2002. (LBNL-50991)

Spycher, N.F. and M.H. Reed. Fugacity Coefficients of H2, CO2, CH4, H2O and of H2O-CO2-CH4 Mixtures: A Virial Equation Treatment for Moderate Pressures and Temperatures Applicable to Calculations of Hydrothermal Boiling, *Geochim. Cosmochim. Acta*, Vol. 52, pp. 739 - 749, 1988.

van Genuchten, M.Th. A Closed-Form Equation for Predicting the Hydraulic Conductivity of Unsaturated Soils, *Soil Sci. Soc. Am. J.*, Vol. 44, pp. 892 - 898, 1980.

Verma, A. and K. Pruess. Thermohydrologic Conditions and Silica Redistribution Near High-Level Nuclear Wastes Emplaced in Saturated Geological Formations, *Journal of Geophysical Res.*, 93 (B2), pp. 1159-1173, 1988.

APPENDIX A. Test Problem 3: Radial Flow from a CO2 Injection Well[&]

1. INTRODUCTION AND GENERAL DESCRIPTION

This problem addresses two-phase flow of CO2 and water for simplified flow geometry and medium properties. The aquifer into which injection is made is assumed infinite-acting, homogenoeus, and isotropic. Gravity and inertial effects are neglected, injection is made at a constant mass rate, and flow is assumed 1-D radial (line source). Under the conditions stated the problem has a similarity solution where dependence on radial distance R and time t occurs only through the similarity variable $\xi = R^2/t$ (O'Sullivan 1981; Doughty and Pruess 1992).

2. LIST OF PROCESSES BEING STUDIED

Two-phase flow of CO2 and water subject to relative permeability and capillary effects.
Change of fluid density, viscosity, and CO2 solubility with pressure and salinity.
Formation dry-out with precipitation of salt.

3. DEFINITION OF THE PROBLEM AND INPUT DATA

Problem parameters are summarized in Tables A.1 and A.2.

4. PROBLEM VARIATIONS

Neglect salinity of the aqueous phase. Include non-isothermal effects. Include permeability changes due to precipitation. Inject gas that is 50 % CO2, 50 % N2.

5. DEFINITION OF RESULTS TO BE CALCULATED

Data on CO2 and brine density and viscosity, and CO2 solubility, for the range of thermodynamic conditions encountered in the problem. Gas saturation, dissolved CO2 mass fraction, fraction of void space containing precipitated salt, and fluid pressure as functions of the similarity variable $\xi = R^2/t$. (Use both profiles at constant time and time-series data at a specific location for plotting.)

6. COMPARISON CRITERIA

Results should match within +/- 5 %.

7. REFERENCES

Corey, A.T. The Interrelation Between Gas and Oil Relative Permeabilities, *Producers Monthly*, pp. 38 - 41, November 1954.

[&] proposed by Karsten Pruess; e-mail: K_Pruess@lbl.gov

Doughty, C. and K. Pruess. A Similarity Solution for Two-Phase Water, Air and Heat Flow Near a Linear Heat Source in a Porous Medium, *J. of Geophys. Res.*, 97 (B2), 1821-1838, 1992.

O'Sullivan, M.J. A Similarity Method for Geothermal Well Test Analysis, *Water Resour. Res.*, Vol. 17, No. 2, pp. 390 – 398, 1981.

van Genuchten, M.Th. A Closed-Form Equation for Predicting the Hydraulic Conductivity of Unsaturated Soils, *Soil Sci. Soc. Am. J.*, Vol. 44, pp. 892 - 898, 1980.

Table A.1 Hydrogeologic parameters.

Permeability Porosity Pore compressibility Aquifer thickness	$k = 10^{-13}\ m^2$ $\phi = 0.12$ $c = 4.5x10^{-10}\ Pa^{-1}$ 100 m
Relative permeability	
liquid: van Genuchten function (1980) $k_{rl} = \sqrt{S^*}\left\{1-\left(1-\left[S^*\right]^{1/\lambda}\right)^{\lambda}\right\}^2$ irreducible water saturation exponent	$S^* = (S_l - S_{lr})/(1 - S_{lr})$ $S_{lr} = 0.30$ $\lambda = 0.457$
gas: Corey curve (1954) $k_{rg} = \left(1-\hat{S}\right)^2\left(1-\hat{S}^2\right)$ irreducible gas saturation	$\hat{S} = \dfrac{(S_l - S_{lr})}{(1 - S_{lr} - S_{gr})}$ $S_{gr} = 0.05$
Capillary pressure	
van Genuchten function (1980) $P_{cap} = -P_0\left(\left[S^*\right]^{-1/\lambda} - 1\right)^{1-\lambda}$ irreducible water saturation exponent strength coefficient	$S^* = (S_l - S_{lr})/(1 - S_{lr})$ $S_{lr} = 0.0$ $\lambda = 0.457$ $P_0 = 19.61$ kPa

Table A.2 Initial conditions and injection specifications

Pressure	120 bar
Temperature	45 ˚C
Salinity	15 wt.-% NaCl
CO2 injection rate	100 kg/s

APPENDIX B. Test Problem 4: CO2 Discharge Along a Fault Zone*

1. INTRODUCTION AND GENERAL DESCRIPTION

This problem explores CO2 loss from storage through a leaky fault, using a highly simplified 1-D linear flow geometry. It is envisioned that an aquifer into which CO2 disposal is made is intersected by a vertical fault, which establishes a connection through an otherwise impermeable caprock to another aquifer 500 m above the storage aquifer (Fig. B.1a). This situation is idealized by assuming 1-D flow geometry and constant pressure boundary conditions as shown in Fig. B.1b (Pruess and García, 2000).

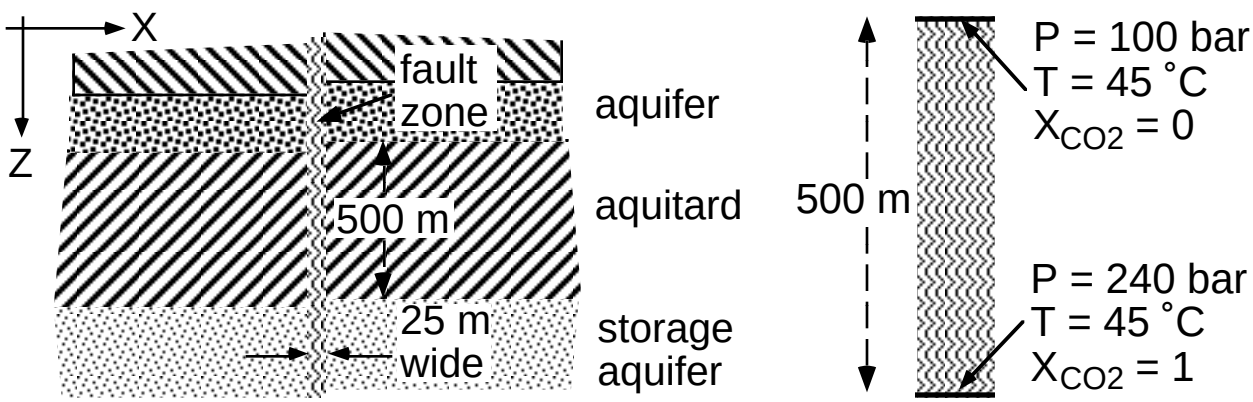

(a) (b)

Figure B.1 Schematic of the fault zone model (a) and applied boundary conditions (b).

2. LIST OF PROCESSES BEING STUDIED

Immiscible displacement of water by CO2 subject to pressure, gravity, and capillary pressure effects.

Change of fluid density, viscosity, and CO2 solubility with pressure.

Formation dry-out.

3. DEFINITION OF THE PROBLEM AND INPUT DATA

Hydrogeologic parameters are identical to those of problem 3 (Table A.1), except that porosity is increased to 35 %. The fault zone is assumed to be 25 m wide and 500 m tall, with boundary conditions as given in Fig. D.1b. The reservoir fluid is assumed to be pure water (no salinity). Initial conditions are pressures in hydrostatic equilibrium relative to P = 100 bar at the top; temperature is held constant at T = 45 ˚C throughout.

---

* proposed by Karsten Pruess; e-mail: K_Pruess@lbl.gov

4. PROBLEM VARIATIONS

Include salinity of the aqueous phase and permeability changes due to precipitation. Include non-isothermal effects. Assume gas composition is 50 % CO_2, 50 % N_2.

5. DEFINITION OF RESULTS TO BE CALCULATED

Data on CO_2 and water density and viscosity, and CO_2 solubility, for the range of thermodynamic conditions encountered in the problem. Vertical profiles of gas saturation, fluid pressure, and dissolved CO_2 mass fraction at different times. CO_2 inventory in gas and liquid phases after 10^7 seconds. Mass flow rates of CO_2 at the bottom and of water at the top vs. time (normalized for a 1 m thick section).

6. COMPARISON CRITERIA

Results should match to with +/- 5 %.

7. REFERENCES

Pruess, K. and J. García. Multiphase Flow Dynamics During CO_2 Injection into Saline Aquifers, submitted to *Environmental Geology*, September 2000.

APPENDIX C. Test Problem 7: CO_2 Injection into a 2-D Layered Brine Formation[#]

1. INTRODUCTION AND GENERAL DESCRIPTION

This test problem is patterned after the CO_2 injection project at the Sleipner Vest field in the Norwegian sector of the North Sea, and is intended to investigate the dominant physical processes associated with the injection of supercritical CO_2 into a layered medium. Significant simplifications have been made, the most important of which is the assumption of isothermal conditions (37 ˚C, the ambient temperature of the formation). CO_2 injection rates (1,000,000 tonnes per year), system geometry, and system permeabilities correspond approximately to those at Sleipner, although no attempt was made to represent details of the permeability structure within the host formation. Injection of the supercritical CO_2, which is less dense than the saline formation waters into which it is injected, causes it to rise through the formation. Its rate of ascent, however, is limited by the presence of four relatively low permeability shales. The top and bottom of the formation is assumed to be impermeable. The only reactive chemistry considered in this problem is the dissolution of CO_2 in the aqueous phase.

2. LIST OF PROCESSES BEING STUDIED

a) Gravity-driven advection in response to strong vertical and lateral density gradients induced by the injection of CO_2 into saline formation water.
b) Density, viscosity, and solubility formulations of water and CO_2 as a function of pressure and temperature (P and T).

3. DEFINITION OF THE PROBLEM AND INPUT DATA

System Geometry:

The system is idealized as a two dimensional symmetric domain perpendicular to the horizontal injection well which has a screen length of 100 meters (Figure C.1). A one meter thick section perpendicular to the horizontal well is considered. The thickness of the formation at the injection site is 184 meters. The injection point is 940 meters below the sea floor, while the ocean depth at the site is 80 meters. The formation is assumed to consist of four lower permeability shale units 3 meters thick which are distributed within the high permeability sand. Each shale unit is separated by 30 meters. The well is 30 meters below the lowest shale unit, while the bottom of the aquifer is another 22 meters below the well.

[#] proposed by Carl Steefel; e-mail: steefel1@llnl.gov

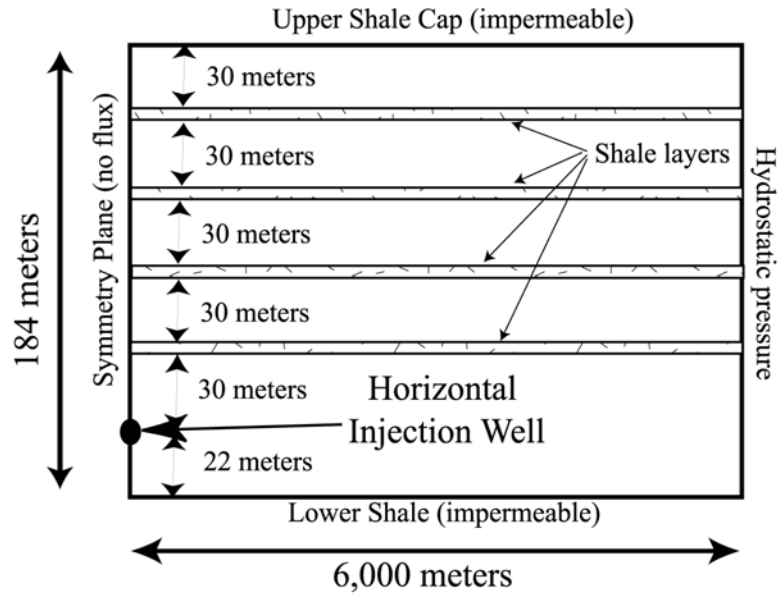

Figure C.1 Schematic representation of geometry for CO2 injection in Utsira Formation.

Boundary conditions:

No heat or mass flux is allowed across any of the boundaries except the vertical boundary 6,000 meters from the injection well. This boundary is fixed at hydrostatic pressure, thus allowing flow into and out of the domain so as to avoid overpressuring the formation. The 6,000 meter boundary is chosen, however, to be far enough from the injection well that the CO_2 does not reach this boundary after 2 years of injection.

Initial conditions (Table C.1):

a) T = 37 ˚C (isothermal throughout)
b) P = hydrostatic (approximately 110 bars at injection point, approximately 90 bars at top of formation).
c) CO_2 in the aqueous phase in equilibrium with a P_{CO2} of 0.5 bars, a typical value for sedimentary formation waters at the temperature we are considering.

Table C.1 Initial conditions and injection specifications

Pressure at well	110 bar
Temperature	37 ˚C
Salinity	3.2 wt.-% NaCl
CO2 injection rate	0.1585 kg/s in half space

Injection specifications (Table C.1):

a) Temperature = 37 ˚C
b) Injection rate: 31.7 kg/s over entire screen length (100 meters), corresponding to 0.317 kg/s for the 1 meter thick section considered. Because of symmetry, injection rate in half space is therefore 0.1585 kg/s.
c) Height of well cell: 1 meter.
d) Injection time scale: 2 years

Input data (Table C.2):

a) Capillary pressure and relative permeability described with van Genuchten parameters (both liquid and gas mobile). Porosity is 35% for sands, 10.25 % for shales.
b) Fully saturated permeability ($k = 3 \times 10^{-12}$ m^2 in sand layers, $10^{-14} m^2$ in shales)
c) Density, viscosity, and solubility in water of CO_2 as functions of P and T (Span and Wagner, 1996).
d) Vapor-liquid equilibrium properties of water.

4. PROBLEM VARIATIONS

Include non-isothermal effects by making the CO_2 injection temperature equal to 65 ˚C.

5. RESULTS TO BE CALCULATED

Liquid and gas saturations as a function of space and time. CO_2 concentration in the aqueous phase as a function of space. Gas and liquid fluxes.

6. COMPARISON CRITERIA

Results should match within +/- 5%.

Table C.2 Hydrogeologic parameters

Permeability Porosity Aquifer thickness	Sands: 3×10^{-12} m^2; Shales: 10^{-14}m^2 Sands: $\phi = 0.35$; Shales: $\phi = 0.1025$ 184 m
Relative permeability	
liquid: van Genuchten function (1980) $k_{rl} = \sqrt{S^*}\left\{1-\left(1-\left[S^*\right]^{1/\lambda}\right)^{\lambda}\right\}^2$ irreducible water saturation exponent	$S^* = \left(S_l - S_{lr}\right)/\left(1 - S_{lr}\right)$ $S_{lr} = 0.20$ $\lambda = 0.400$
gas: van Genuchten function (1980) $k_{rg} = \sqrt{S_g^*}\left\{1-\left(1-\left[S_g^*\right]^{1/\lambda}\right)^{\lambda}\right\}^2$ irreducible gas saturation exponent	$S_g^* = \left(S_g - S_{gr}\right)/\left(1 - S_{gr}\right)$ $S_{gr} = 0.05$ $\lambda = 0.400$
Capillary pressure	
van Genuchten function (1980) $P_{cap} = -P_0\,([S^*]^{-1/\lambda} - 1)^{1-\lambda}$ irreducible water saturation exponent strength coefficient	$S^* = \left(S_l - S_{lr}\right)/\left(1 - S_{lr}\right)$ $S_{lr} = 0.20$ $\lambda = 0.400$ Sand: $P_0 = 3.58$ kPa; Shale: $P_0 = 62.0$ kPa

7. REFERENCES

van Genuchten, M.Th. A Closed-Form Equation for Predicting the Hydraulic Conductivity of Unsaturated Soils, *Soil Sci. Soc. Am. J.*, Vol. 44, pp. 892 - 898, 1980.

Span, R. and W. Wagner. A New Equation of State for Carbon Dioxide Covering the Fluid Region from the Triple-Point Temperature to 100 K at Pressures up to 800 MPa, *J. Phys. Chem. Ref. Data*, Vol. 25, No. 6, pp. 1509 - 1596, 1996.